Glycyrrhizic acid attenuates corneal inflammation and pathological angiogenesis through FAK/PI3K/AKT signaling

JINJIN YU[1,2], HUIHENG QU[3,4], YINMING FANG[2], WEICHENG XU[2], NANNAN DING[5], JIE JI[1], NAN WANG[4,6] and WEI SHI[2]

[1]Department of Ophthalmology, Wuxi Affiliated Hospital of Nanjing University of Chinese Medicine, Wuxi, Jiangsu 214000, P.R. China; [2]Department of Ophthalmology, Nanjing Hospital Affiliated to Nanjing University of Chinese Medicine, The First Clinical Medical College of Nanjing University of Chinese Medicine, Nanjing, Jiangsu 210003, P.R. China; [3]Department of General Surgery, Jiangnan University Medical Center, Jiangnan University, Wuxi, Jiangsu 214002, P.R. China; [4]Department of Cancer Biology, Atrium Health Wake Forest Baptist Comprehensive Cancer Center, Winston-Salem, NC 27157, USA; [5]Department of Ophthalmology, Jiangnan University Medical Center, Jiangnan University, Wuxi, Jiangsu 214002, P.R. China; [6]Department of Breast Surgery, Tianjin Medical University Cancer Institute and Hospital, Key Laboratory of Cancer Prevention and Therapy, National Clinical Research Center for Cancer, Tianjin 300060, P.R. China

Received May 28, 2026; Accepted September 18, 2026

DOI: 10.3892/mmr.2026.14046

Abstract. Corneal alkali burns lead to severe inflammation and corneal neovascularization (CNV), both of which are major causes of visual impairment. The suppression of inflammation, promotion of epithelial repair and inhibition of CNV formation are promising therapeutic strategies for restoring corneal transparency. This study investigated the effects and underlying mechanisms of glycyrrhizic acid (GA) on inflammation, epithelial wound healing and CNV in a murine model of alkali burn. GA markedly alleviated corneal opacity, enhanced epithelial wound closure and reduced CNV formation in alkali-burned mice. Mechanistically, GA markedly downregulated tumor necrosis factor-α, interleukin (IL)-6, IL-17 and vascular endothelial growth factor A (VEGF-A) expression in injured corneas. In human umbilical vein endothelial cells, GA attenuated VEGF-A-induced proliferation and angiogenic activity. In human corneal epithelial cells, GA activated the focal adhesion kinase (FAK)/PI3K/AKT signaling pathway, upregulated Bcl-2 and cyclin D1 expression and suppressed Bax and caspase-3 expression, thereby promoting cell proliferation and reducing apoptosis. Overall, GA exerts protective effects against alkali burn-induced corneal injury by suppressing inflammation and neovascularization while promoting epithelial repair through activation of the FAK/PI3K/AKT signaling pathway.

Correspondence to: Professor Wei Shi, Department of Ophthalmology, Nanjing Hospital Affiliated to Nanjing University of Chinese Medicine, The First Clinical Medical College of Nanjing University of Chinese Medicine, 155 Hanzhong Road, Qinhuai, Nanjing, Jiangsu 210003, P.R. China
E-mail: fsyy01096@njucm.edu.cn

Dr Nan Wang, Department of Breast Surgery, Tianjin Medical University Cancer Institute and Hospital, Key Laboratory of Cancer Prevention and Therapy, National Clinical Research Center for Cancer, Building B, Huanhu West Road, Tiyuanbei Road, Hexi, Tianjin 300060, P.R. China
E-mail: 9820211029@nankai.edu.cn

Key words: glycyrrhizic acid, corneal neovascularization, corneal epithelial repair, inflammation, focal adhesion kinase/PI3K/AKT signaling pathway

Introduction

Corneal blindness is a major contributor to global vision loss (1). Among its etiologies, corneal opacity and corneal neovascularization (CNV) secondary to inflammation are the major pathological features responsible for visual impairment. Corneal inflammation and neovascularization often occur secondary to various diseases, including severe dry eye, chemical burns, infectious keratitis, corneal graft rejection and other conditions (2-5).

Oxidative stress, inflammation and CNV are the primary contributors to corneal structural disruption and visual deterioration, although the underlying mechanisms remain poorly understood. Excessive inflammation is a key determinant of poor prognosis. After injury, neutrophils, monocytes and lymphocytes are recruited to the lesion site where they release pro-inflammatory cytokines, such as IL-1β, IL-6, tumor necrosis factor-α (TNF-α), nuclear factor-κB (NF-κB) and vascular endothelial growth factor A (VEGF-A), which further promote corneal ulceration and neovascular formation. Therefore, suppressing inflammatory progression is crucial for the management of alkali burn-induced corneal injury (6). Currently, topical corticosteroids and nonsteroidal anti-inflammatory drugs combined with epithelial healing-promoting eye drops remain the standard therapeutic approach (7,8).

Glycyrrhizic acid (GA), a triterpenoid saponin derived from *Glycyrrhiza uralensis* (licorice root), possesses diverse pharmacological properties, such as anti-inflammatory, antiviral, antitumor and immunomodulatory activities (9). Pharmacological studies have demonstrated that GA exerts glucocorticoid-like activities by specifically inhibiting 11β-hydroxysteroid dehydrogenase, an enzyme responsible for regulating systemic cortisol levels (10). Due to its limited water solubility, GA is clinically applied in salt form, such as dipotassium glycyrrhizinate (DG) or monoammonium glycyrrhizinate. GA derivative-containing eye drops are widely used in ophthalmology to manage various ocular surface disorders, such as dry eye, itching, foreign-body sensation and allergic conjunctivitis (11). A previous study showed that GA alleviates inflammation and oxidative stress in corneal epithelial cells and diabetic corneal models (12). DG-baicalin nanomicelle eye drops promote corneal epithelial and nerve regeneration in diabetic mice. This effect is mediated through the downregulation of high-mobility group box 1 (HMGB1), its receptors, receptor for advanced glycation and products and Toll-like receptor 4 and the inflammatory mediators interleukin (IL)-1β and IL-6 (13). Moreover, a previous clinical pilot study demonstrated that topical administration of 25 mg/ml glycyrrhizin eye drops for 28 days effectively improved symptoms in patients with moderate-stage dry eye, showing good tolerability (14). Nevertheless, the precise mechanisms underlying the protective effects of GA on corneal injury have not yet been fully elucidated.

The corneal alkali-burn model is a well-established experimental system for investigating ocular surface inflammation and neovascularization, characterized by marked inflammatory infiltration, CNV and stromal fibrosis (15). Topical corticosteroids, such as dexamethasone (Dex), are used during the acute phase to suppress inflammation and promote tissue recovery (16). However, prolonged or repeated corticosteroid use can cause adverse effects, including elevated intraocular pressure and corneal melting (17). Given its glucocorticoid-like anti-inflammatory properties and reduced side effects, GA may serve as a natural alternative to corticosteroids for the treatment of corneal injury.

Therefore, the present study aimed to investigate the protective effects of GA in an NaOH-induced corneal alkali-burn model, focusing on its roles in promoting corneal epithelial repair, inhibiting CNV and reducing inflammatory responses, as well as to elucidate the potential involvement of the focal adhesion kinase (FAK)/PI3K/AKT pathway in these processes.

Materials and methods

Cell culture. Human umbilical vein endothelial cells (HUVECs; CTCC-003-0025) and human corneal epithelial cells (HCECs; cat. no. NCL-10051) were purchased from Mesien CTCC (Zhejiang Meisen Cell Technology Co., Ltd.). HUVECs were cultured in endothelial cell medium (ECM; cat. no. 1001; ScienCell Research Laboratories, Inc.) supplemented with 10% fetal bovine serum (FBS; cat. no. A52556701; Gibco; Thermo Fisher Scientific, Inc.) and 1% penicillin-streptomycin (cat. no. P1400; Beijing Solarbio Science & Technology Co., Ltd.). HCECs were maintained in keratinocyte serum-free medium (Keratinocyte-SFM; Invitrogen; Thermo Fisher Scientific, Inc.) supplemented with 10% FBS, 5 ng/ml epidermal growth factor (cat. no. HY-P7109; MedChemExpress), 0.005 mg/ml insulin (cat. no. 11070-73-8; Merck KGaA), 0.05 mg/ml bovine pituitary extract, 500 ng/ml hydrocortisone and 1% penicillin-streptomycin. All cells were incubated at 37˚C in a humidified 5% CO_2 atmosphere. The PI3K inhibitor, LY294002 (cat. no. HY-10108; MedChemExpress), was applied to pretreat cells at a final concentration of 10 μM for 2 h before subsequent NaOH and GA treatment to block PI3K/AKT signaling (18).

Cell viability assay. Cell viability/proliferation was assessed using a Cell Counting Kit-8 (CCK-8) (cat. no. CK-04; Dojindo Laboratories, Inc.). Briefly, HUVECs were seeded into 96-well plates at $5x10^3$ cells/well and treated with VEGF-A or VEGF-A plus GA for 48 h, followed by the addition of 10 μl CCK-8 reagent/well and incubation for 1-2 h. Optical density (OD) was measured at 450 nm. HCECs were exposed to 6 mM NaOH for 50 sec, washed with phosphate-buffered saline (PBS; cat. no. BL302A; Biosharp Life Sciences), cultured for 24 h and analyzed with a CCK-8, as aforementioned for HUVECs.

Western blotting. Cells and tissues were lysed using RIPA buffer (cat. no. P0013B; Beyotime Biotechnology) supplemented with protease and phosphatase inhibitors. Protein concentrations were determined using a bicinchoninic acid assay kit (cat. no. 23225; Thermo Fisher Scientific, Inc.). After protein quantification, 10-20 μg total protein/lane was loaded, mixed with 5X loading buffer, heated at 95˚C for 5 min and subsequently separated via 10% SDS-PAGE). Proteins were then transferred to polyvinylidene fluoride membranes (cat. no. IPVH00010; MilliporeSigma). After blocking with 5% nonfat milk (1 h, 23-25˚C), the membranes were incubated overnight at 4˚C with primary antibodies (Table I). After washing with PBS containing 0.1% Tween 20, the membranes were incubated with horseradish peroxidase (HRP)-conjugated secondary antibodies (Bioss, detailed catalogue number and dilution ratio listed in Table I) for 2 h at room temperature. β-actin was used as the reference protein and loading control for normalization. The signals were visualized using an enhanced chemiluminescence system (cat. no. 34096; Thermo Fisher Scientific, Inc.) and imaged with an Amersham imaging platform (GE Healthcare). Band intensities were quantified using ImageLab software (v.6.1; Bio-Rad Laboratories, Inc.).

Cell migration assay. Cell migration was assessed using Transwell chambers (8-μm pore size). HUVECs pretreated for 48 h with VEGF-A alone or in combination with GA were resuspended in serum-free DMEM and seeded into the upper chambers at $2x10^4$ cells/well. The lower chambers received 800 μl complete medium (containing 10% FBS) as the chemoattractant. After a 48-h incubation, the migrated cells were fixed with 1% paraformaldehyde (PFA) at room temperature (for 20 min, stained with Giemsa at room temperature for 15 min and quantified via light microscopy.

EdU proliferation assay. HCECs seeded on coverslips in 24-well plates at a density of $2x10^4$ cells/well. Cells were

Table I. Antibodies.

Antibody	Supplier	Dilution	Catalogue number
PI3K P85 alpha	Affinity Biosciences	1:1,000	AF6241
Phosphorylated PI3K P85 alpha (Tyr607)	Affinity Biosciences	1:1,000	AF3241
AKT	Affinity Biosciences	1:1,000	AF6261
Phosphorylated pan-AKT1/2/3 (Ser473)	Affinity Biosciences	1:1,000	AF3263
FAK	Proteintech Group, Inc.	1:5,000	12636-1-AP
Phosphorylated FAK (Tyr397)	Proteintech Group, Inc.	1:1,000	83933-1-RR
VEGF-A (for WB)	Proteintech Group, Inc.	1:5,000	81323-2-RR
VEGF-A (for IHC)	Affinity Biosciences	1:200	AF5131
Bax	Affinity Biosciences	1:1,000	AF0120
Bcl-2	Affinity Biosciences	1:1,000	AF6139
Caspase-3	Affinity Biosciences	1:1,000	AF6311
Cyclin D1	Affinity Biosciences	1:1,000	AF0931
Beta-actin	Affinity Biosciences	1:5,000	AF7018
HRP-conjugated Goat Anti Rabbit IgG (H+L)	BIOSS	1:5,000	bs-0295G
HRP-conjugated Goat Anti Mouse IgG (H+L)	BIOSS	1:5,000	bs-0296G

incubated with 10 μM EdU at 37˚C for 2 h, fixed in 4% paraformaldehyde 15 min at room temperature, permeabilized with 0.3% Triton X-100 in PBS for 10 min at room temperature, then reacted with Click-iT reaction solution for 30 min at room temperature in the dark. Nuclei were counterstained with 1X Hoechst 33342 for 10 min at room temperature. Fluorescence images were acquired using a fluorescence microscope. For quantitative analysis, at least five random fields of view were captured for each group, and EdU-positive cell ratio was quantified with ImageJ software (v1.53; National Institutes of Health). The assay was performed using the BeyoClick EdU-594 Cell Proliferation Detection Kit (C0078S, Beyotime, China) following the manufacturer's instructions.

Tube formation assay. HUVECs ($2x10^3$ cells/well) were seeded into 96-well plates precoated with Matrigel (cat. no. 354234; Corning Inc.) and incubated in a medium containing VEGF-A or VEGF-A plus GA at 37˚C for 12 h to induce capillary-like structures. Images were captured with a Nikon TS2 inverted microscope (Nikon Corporation). Tube formation was analyzed by measuring length and branch points using ImageJ software (v.1.53; National Institutes of Health).

Flow cytometric analysis of apoptosis. Apoptosis was evaluated using the FITC Annexin V Apoptosis Detection Kit I (cat. no. 556547; BD Biosciences). Cells were washed twice with PBS, resuspended in 100 μl of 1X binding buffer and stained with 5 μl each of FITC Annexin V and propidium iodide at room temperature for 15 min in the dark, following the manufacturer's instructions. Subsequently, 400 μl binding buffer was added and the samples immediately subjected to flow cytometric analysis using BD FACSCanto II flow cytometer (BD Biosciences). The data were analyzed using FlowJo software (v.10.8; BD Biosciences). The apoptotic rate was calculated as the sum of the percentage of early (Annexin V^+/PI^-, Q1-LR) and late apoptotic cells (Annexin V^+/PI^+, Q1-UR).

Mouse corneal alkali-burn model. All animal procedures were reviewed and approved by the Animal Ethics Committee of the Wuxi Affiliated Hospital of Nanjing University of Chinese Medicine (Wuxi, China; approval no. 2024-171-01) and complied with Chinese regulations on animal welfare and the ARVO Statement for the Use of Animals in Ophthalmic and Vision Research. C57BL/6J mice (male, 8 weeks old; weight 20-22 g) were purchased from GemPharmatech Co., Ltd. A total of 120 mice were randomly assigned to six groups (n=20 per group) for this *in vivo* study. All animals were housed and maintained under standard conditions (20-26˚C; 30-70% humidity; 12-h light/dark cycle) with food and water provided *ad libitum*. Following acclimation, an alkali burn-induced corneal injury model was established as previously described (19,20). The mice were anesthetized by intraperitoneal injections of ketamine (80 mg/kg) and xylazine (16 mg/kg), followed by a topical application of 0.5% proparacaine to the right eye. Subsequently, a 2-mm-diameter circular filter paper soaked in 1 N NaOH (cat. no. 484024; Merck KGaA) was placed on the central cornea of the right eye for 30 sec. The ocular surface was then thoroughly irrigated with PBS for 1 min to remove residual alkali. On day 14 after injury, the mice were anesthetized by intraperitoneal administration of ketamine (80 mg/kg) and xylazine (16 mg/kg) and then sacrificed by gradual-fill CO_2 inhalation at a displacement rate of 20% of the chamber volume per minute. CO_2 exposure was continued for 5 min. Following CO_2 exposure, the mice were continuously observed for at least 3 min, during which the absence of spontaneous respiration and heartbeat was confirmed. The pedal withdrawal reflex and the corneal reflex of the unaffected eye were subsequently assessed. Cervical dislocation was then performed as a secondary physical method to ensure death before eyeball enucleation.

Clinical evaluation. A total of 120 mice were randomly assigned to six groups (n=20/group): normal, PBS, low-dose GA (0.5 mg/ml), medium-dose GA (1 mg/ml), high-dose GA

Table II. Clinical scoring criteria for corneal opacity and neovascularization following alkali burn.

Criteria	Corneal lesions as examined under a slit-lamp microscope	Score
Corneal opacity	Clear	0
	Slight haze, iris clearly visible	1
	Moderate haze, iris blurred but visible	2
	Severe haze, iris barely discernible	3
	Total opacity, iris invisible	4
Corneal neovascularization extent	None	0
	Confined to limbus	1
	Extending toward central cornea	2
	Reaching the central cornea	3
Neovascular density	None	0
	Only microscopically visible	1
	Clearly visible microscopically	2
	Visible to the naked eye	3

(2 mg/ml) and positive control (1 mg/ml Dex) groups. Mice were divided into two batches. The first batch (n=8/group) was used for *in vivo* clinical evaluation and immunohistochemistry (IHC) and the second batch (n=12/group) sacrificed for other histological and molecular analyses, with a total of 20 mice/group. The normal group was not subjected to alkali burn-induced corneal injury and only treated with PBS. All other groups were subjected to alkali burn-induced corneal injury and treatments. Each eye received 10 μl eye drops 4 times daily for 14 consecutive days. Corneal lesions were examined under a slit-lamp microscope on days 3, 7 and 14 after injury (day 0=model induction) and scored for corneal opacity, CNV extent and neovascular density, as shown in Table II (7).

Histology and IHC. On day 14, mice were humanely sacrificed and their right eyeballs enucleated and fixed in 4% PFA at 4˚C overnight. Tissues were washed with PBS, dehydrated through graded ethanol, cleared, paraffin-embedded and sectioned at a thickness of 4 μm. Tissue sections were stained with hematoxylin-eosin (H&E) at room temperature for 5 (hematoxylin) and 2 min (eosin) for histological evaluation and IHC for protein expression analysis. For IHC, the paraffin-embedded sections were deparaffinized, rehydrated and permeabilized with 0.1% Triton X-100 for 15 min. Nonspecific binding was blocked using 10% goat serum (Wuhan Servicebio Technology Co., Ltd.) for 2 h at 25˚C. To quench endogenous peroxidase activity, the sections were treated with 3% H_2O_2 in methanol for 15 min at room temperature and subsequently incubated with a primary antibody against VEGF-A (1:200; cat. no. AF5131; Affinity Biosciences) at 4˚C for 12 h. After washing with PBS, the sections were incubated with an HRP-conjugated secondary antibody (1:200; cat. no. GB23301; Wuhan Servicebio Technology Co., Ltd.) for 60 min at 37˚C. Immunoreactive signals were visualized using DAB. Sections were counterstained with hematoxylin at room temperature for 2 min. Microscopy was performed using a light microscope (Nikon Corporation). The central corneal thickness and average OD of the IHC signals were assessed and quantified using ImageJ (v.1.53; National Institutes of Health).

Corneal whole-mount immunofluorescence. Mice were sacrificed on day 14 post-alkali burn and their eyes enucleated via blunt dissection. Briefly, the eyelids were retracted using the thumb and index finger, followed by the placement of forceps beneath the globe. The forceps were then closed and used to gently extract the eyeball from the orbit. The enucleated eyes were fixed in 4% PFA at 4˚C overnight. After PBS washes, the corneas were transferred to a primary antibody solution and incubated at 4˚C for three days. The solution was prepared in 1X PBS containing 1% bovine serum albumin, 0.1% Triton X-100 and the following antibodies: Dylight 550-conjugated anti-PECAM-1/CD31 (1:100, cat. no. AF6191; Affinity Biosciences) and Alexa Fluor 488-conjugated anti-LYVE-1 (1:100, cat. no. AF4202; Affinity Biosciences). Following incubation, the corneas were washed three times with 1x PBS for 20 min each. Whole-mount images were captured using a laser confocal microscope (LSM700; Carl Zeiss AG) and the fluorescence intensities of CD31 and LYVE-1 quantified using ImageJ (v.1.53; National Institutes of Health). CD31 is highly expressed on the vascular endothelial cells of nascent and mature blood vessels, whereas LYVE-1 labels lymphatic endothelial cells and is used to assess lymphangiogenesis (15).

Western blotting analysis. For protein extraction from corneal tissues, the aforementioned western blotting workflow was adopted. Briefly, harvested corneal tissues were fully homogenized in RIPA lysis buffer supplemented with protease and phosphatase inhibitors prior to protein quantification. GAPDH was selected as the loading control for corneal tissue lysates, whereas β-actin served as the internal reference for cell samples. The procedures of SDS-PAGE, membrane transfer, antibody incubation, ECL detection and band intensity quantification were consistent between cells and tissues. Detailed information of all primary antibodies is summarized in Table I.

RNA extraction and reverse transcription-quantitative (RT-q) PCR. Following extraction with TRIzol® reagent (cat. no. 15596018; Thermo Fisher Scientific, Inc.), RNA quality was verified using a NanoDrop spectrophotometer

(A260/A280; NanoDrop Technologies; Thermo Fisher Scientific, Inc.). A reverse transcription kit (cat. no. R433; Vazyme Biotech Co., Ltd.) was used to synthesize cDNA from total RNA with incubation at 50˚C for 5 min and inactivation at 85˚C for 5 sec. For qPCR, reactions containing SYBR Green Master Mix (cat. no. Q711; Vazyme Biotech Co., Ltd.) were run on a CFX96 real-time PCR system (Bio-Rad Laboratories, Inc.) under the following conditions: 95˚C for 30 sec, then 40 cycles of 95˚C for 10 sec and 60˚C for 30 sec, followed by melting curve analysis. Relative expression ($2^{-\Delta\Delta Cq}$) was calculated using *GAPDH* as the internal control. The primer sequences used for RT-qPCR analysis were as follows: mouse BAX (NM-007527), F: 5'-AGGATGCGTCCACCAAGAAGC T-3' and R: 5'-TCCGTGTCCACGTCAGCAATCA-3'; mouse BCL2 (NM-009741), F: 5'-CCTGTGGATGACTGAGTACCT G-3' and R: 5'-AGCCAGGAGAAATCAAACAGAGG-3'; mouse caspase-3 (NM-009810), F: 5'-GGAGTCTGACTG GAAAGCCGAA-3' and R: 5'-CTTCTGGCAAGCCATCTC CTCA-3'; mouse-GAPDH (NM-008084), F: 5'-CATCACTGC CACCCAGAAGACTG-3' and R: 5'-ATGCCAGTGAGCTTC CCGTTCAG-3'.

Data-independent acquisition (DIA)-based quantitative proteomics. DIA-based quantitative proteomics was conducted to compare the protein expression profiles of corneal tissues before and after GA treatment. Tissue samples were lysed and digested using an iST sample preparation kit (PreOmics), followed by high-pH reversed-phase fractionation to generate the spectral library. Liquid chromatography-tandem mass spectrometry was performed using an EASY-nLC 1200 system coupled to an Orbitrap Lumos mass spectrometer (Thermo Fisher Scientific, Inc.) equipped with an Acclaim PepMap C18 analytical column (75 μm x25 cm). Peptides were separated over a 120 min linear gradient of 5-35% solvent B (0.1% formic acid in acetonitrile) at a flow rate of 200 nl/min. Data were acquired in positive ion mode via nano-electrospray ionization (nano-ESI), with an electrospray voltage of 2 kV. The ion transfer capillary temperature was set to 320˚C. Raw data were processed against the UniProt database using Spectronaut X (Biognosys AG). Identification thresholds were set at a 1% false discovery rate at both the peptide and protein levels. Differentially expressed proteins (DEPs) were defined by a fold change >1.5 and P-value <0.05. Kyoto Encyclopedia of Genes and Genomes (KEGG) and Gene Ontology (GO) enrichment analyses were conducted to identify key pathways. This high-throughput DIA-based proteomic analysis was performed as an exploratory approach to identify DEPs and pathways associated with GA treatment.

Enzyme-linked immunosorbent assay (ELISA). Levels of TNF-α (cat. no. BMS607-3TEN), IL-6 (cat. no. BMS603-2) and IL-17 (cat. no. BMS6001) were quantified using commercial ELISA kits (Thermo Fisher Scientific, Inc.), according to the manufacturer's instructions. Samples were diluted 1:5 and added to antibody-precoated 96-well plates (100 μl/well) in duplicate, followed by 2 h incubation at room temperature. After washing, the plates were sequentially incubated with Biotin-conjugated detection antibodies and streptavidin-HRP supplied with the kits, each for 2 and 1 h at room temperature, respectively. Color development was achieved using tetramethylbenzidine substrate for 30 min in the dark; the reaction was terminated with stop solution (1 M phosphoric acid) and absorbance measured at 450 nm. Cytokine concentrations were interpolated by comparison with a standard curve generated using the supplied standards.

Network pharmacology and molecular docking. The Simplified Molecular Input Line Entry System and Structure Data Format structures of GA were retrieved from the PubChem database (https://pubchem.ncbi.nlm.nih.gov/). Potential targets were screened using SwissTargetPrediction (https://swisstargetprediction.ch/) and disease-related targets for 'corneal alkali burn' obtained from the GeneCards database (https://www.genecards.org/). The intersection of GA and disease targets was computed in R (v.4.2.1; https://www.r-project.org; The R Foundation, Vienna, Austria). GO and KEGG enrichment analyses were conducted using Bioconductor packages (http://bioconductor.org/packages/limma) to construct a compound-target-pathway-disease network. PubChem and the Protein Data Bank (rcsb.org/) were used to download three-dimensional structures of the compounds and target proteins. Protein structures were preprocessed (such as removal of solvent molecules) with PyMOL (v.2.6.0; https://www.pymol.org; DeLano Scientific), followed by hydrogenation and charge assignment in AutoDock Tools (v.1.5.7; Scripps Research). Docking was performed using AutoDock Vina and visualization achieved with PyMOL and Discovery Studio (BIOVIA).

Statistical analysis. All experiments were repeated thrice. Data are presented as mean ± SD. Statistical analyses were conducted using GraphPad Prism 10 (Dotmatics). The Shapiro-Wilk test was used to assess data normality and Levene's test applied to evaluate the homogeneity of variances. If these assumptions were met, one-way analysis of variance followed by Tukey's post hoc test was performed. $P<0.05$ was considered to indicate a statistically significant difference.

Results

GA attenuates corneal inflammation and neovascularization in alkali burn-induced mice. To evaluate the *in vivo* effects of GA on corneal inflammation and neovascularization, a mouse corneal alkali-burn model was established and administered different concentrations of GA, Dex, or PBS. Slit-lamp microscopy was performed on days 3, 7 and 14 after injury to monitor corneal morphological changes (Fig. 1A). In the PBS group, extensive CNV was observed by day 14, covering nearly the entire cornea, accompanied by severe opacity and vascular congestion in the central pupillary area (Fig. 1B). By contrast, both Dex and GA treatments markedly improved corneal pathology (Fig. 1C). Notably, the high-dose GA group (2 mg/ml) showed a therapeutic efficacy comparable to that of Dex on day 14 (scores, 4.125 vs. 3.125). Gross observations further confirmed these findings: corneal transparency was substantially restored in GA-treated mice, with background details clearly discernible (Fig. 1D). Histological examination supported these observations. H&E staining revealed a significant reduction in inflammatory-cell infiltration within the corneal stroma and restoration of epithelial thickness in

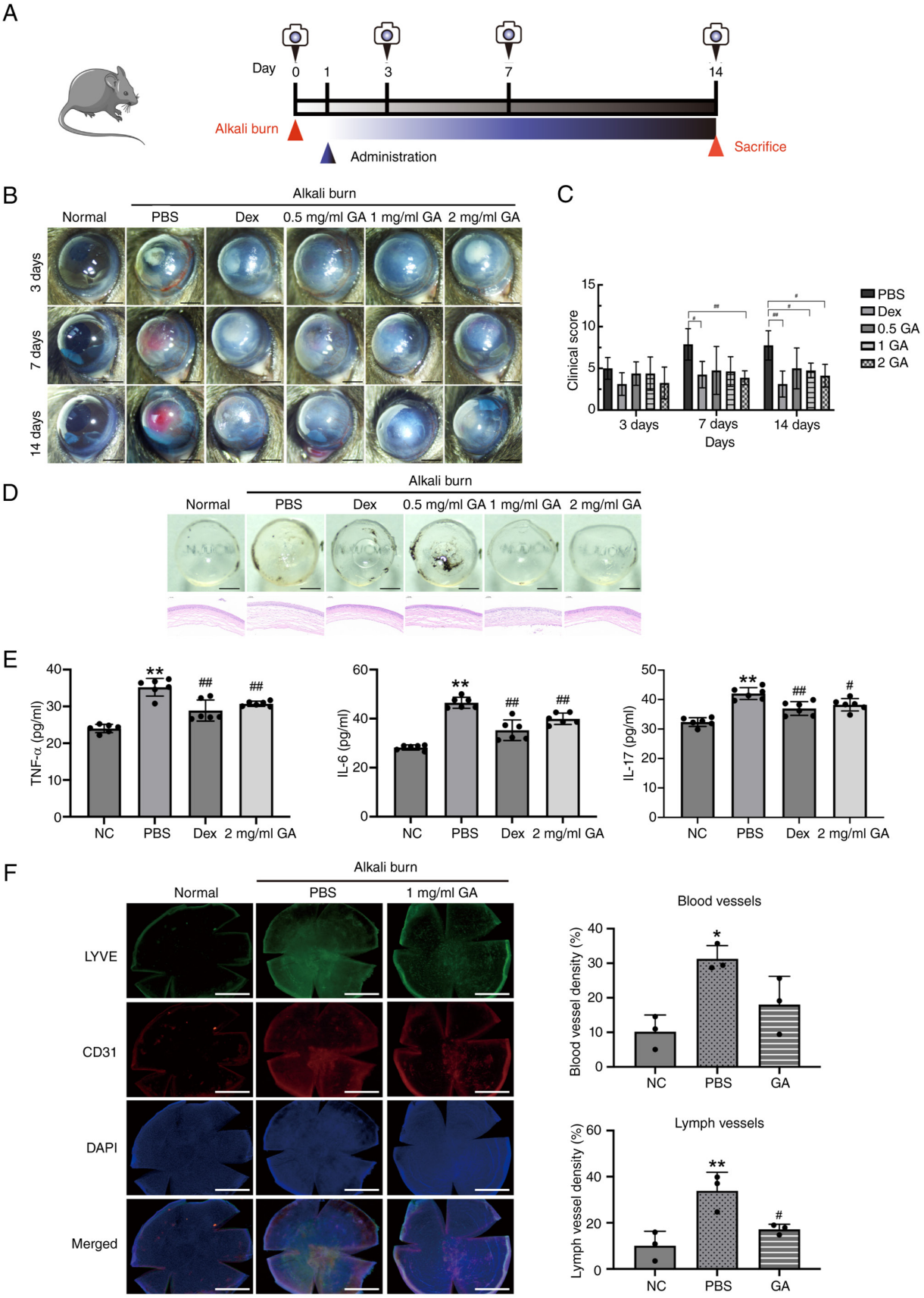

Figure 1. GA ameliorates alkali burn-induced corneal injury. (A) Schematic diagram of the modeling, administration and photographing procedures performed in mice. (B) Images of the anterior ocular segment in the normal, PBS-treated, 1 mg/ml dexamethasone-treated, 0.5 mg/ml GA-treated, 1 mg/ml GA-treated and 2 mg/ml GA-treated groups. (C) Quantitative analysis of the clinical assessment score on days 3, 7 and 14 (n=8). (D) Cornea images on day 14, including hematoxylin-eosin staining images (left; scale bars, 0.05 mm). (E) ELISA results showing the corneal levels of TNF-α IL-6 and IL-17. (F) Immunohistochemistry revealing blood and lymph vessels using the anti-CD31 and anti-LYVE-1 mAbs, respectively. Quantification of the blood and lymph vessel density, as indicated. Data are presented as means ± SD (n=3). ns, not significant; *P<0.05 and **P<0.01 vs. NC group; $^{\#}$P<0.05 and $^{\#\#}$P<0.01 vs. PBS group. GA, glycyrrhizic acid; TNF-α, tumor necrosis factor-α; IL, interleukin.

GA-treated mice compared with those in the model group, suggesting GA exhibits both anti-inflammatory and wound-healing properties.

To further elucidate the anti-inflammatory mechanism of GA, inflammatory cytokine levels in corneal tissues were analyzed. ELISA demonstrated that GA markedly suppressed IL-6, IL-17 and TNF-α expression compared with that in the PBS-treated group (Fig. 1E), indicating that GA alleviated corneal inflammation by inhibiting pro-inflammatory cytokine production. Alkali injury induces pathological corneal angiogenesis and lymphangiogenesis, which are closely associated with elevated inflammatory cytokines (21). Immunofluorescence staining showed that vascular (18.05%) and lymphatic vessel (17.20%) densities in GA-treated corneas were markedly reduced compared with those in the PBS group (31.27 and 33.89%, respectively; Fig. 1F), further confirming that GA effectively inhibits pathological-blood and lymphatic-vessel formation. The present findings highlighted that GA ameliorates alkali burn-induced corneal injury by suppressing inflammatory cytokine expression and pathological angiogenesis, thereby alleviating corneal inflammation and promoting tissue recovery.

GA inhibits VEGF-A-induced proliferation, migration and tube formation in HUVECs. To elucidate the role of GA in angiogenesis, the present study systematically evaluated its effects on VEGF-A-induced proliferation, migration and tube formation in HUVECs. Initially, GA cytotoxicity toward HUVECs was assessed using the CCK-8 assay (Fig. 2B). GA showed no significant effect on cell viability within the concentration range of 0-40 μg/ml. However, a slight inhibitory effect was observed at 80 μg/ml and marked cytotoxicity occurred at 160 μg/ml ($P<0.05$). Accordingly, 80 μg/ml was selected as the working concentration for subsequent experiments. Further results demonstrated that 80 μg/ml GA markedly suppressed VEGF-A-induced HUVEC proliferation, exhibiting an inhibitory effect comparable to that of Dex (Fig. 2C).

Endothelial cell migration is a critical step in angiogenesis (22). Transwell migration assays were employed to evaluate the effect of GA on VEGF-A-stimulated HUVEC migration (Fig. 2D-E). VEGF-A treatment markedly enhanced endothelial cell migration, whereas GA treatment markedly reduced the number of migrated cells. Quantitative analysis confirmed that GA intervention substantially attenuated VEGF-A-induced migratory capacity. The formation of capillary-like tubular networks by endothelial cells is another key phase of angiogenesis (23,24). To further examine the anti-angiogenic potential of GA, Matrigel tube-formation assays were performed (Fig. 2F-H). VEGF-A markedly promoted the formation of complex, highly branched tubular structures, whereas GA treatment markedly reduced tube length, branch points and total lumen numbers, indicating a potent inhibition of angiogenesis. These results indicate that GA effectively suppresses VEGF-A-mediated HUVEC proliferation, migration and tube formation, suggesting that it exerts considerable anti-angiogenic activity *in vitro*.

GA suppresses VEGF-A expression in vivo and in vitro. To investigate the regulatory effect of GA on VEGF-A expression, experiments were performed in HUVECs and a mouse corneal alkali-burn model. Western blotting revealed that GA treatment markedly decreased VEGF-A protein levels in HUVECs compared with that in the control group (Fig. 3A), indicating that GA directly suppresses VEGF-A upregulation in endothelial cells.

Furthermore, IHC and western blotting were performed to examine VEGF-A expression in alkali-burned corneal tissues. IHC results showed that corneas in the PBS group exhibited marked stromal edema and thickening, accompanied by strong VEGF-A immunoreactivity. By contrast, treatment with 2 mg/ml GA markedly reduced VEGF-A expression, with the corneal structure largely preserved (Fig. 3B). Consistently, western blotting analysis confirmed that GA effectively reversed the alkali burn-induced upregulation of VEGF-A expression in corneal tissues (Fig. 3C).

Collectively, these findings demonstrated that GA exerted anti-angiogenic effects *in vivo* and *in vitro* by downregulating VEGF-A expression, thereby inhibiting CNV.

Identification of potential targets of GA and GO/KEGG pathway analyses. To further elucidate the potential molecular mechanisms by which GA exerts its therapeutic effects in alkali-burned corneal tissues, DIA-based quantitative proteomics was performed on corneal samples collected on day 7 after injury. Differential protein expression profiles were compared between the PBS and high-dose GA groups (2 mg/ml). In total, 779 DEPs were identified, including 638 upregulated and 141 downregulated proteins (Fig. 4A). Distribution and expression patterns of the top 20 DEPs are presented in Fig. 4B. GO functional enrichment analysis (Fig. 4C) indicated that these DEPs were mainly enriched in 26 biological process, 19 molecular function and 2 cellular component categories. KEGG pathway enrichment analysis (Fig. 4D) revealed that the top five markedly enriched pathways included 'metabolic pathways', 'complement and coagulation cascades', 'pathways in cancer', the 'PI3K/AKT signaling pathway' and 'human papillomavirus infection'.

Given that corneal alkali burn is typically accompanied by severe inflammation, pathological neovascularization, corneal ulceration and loss of transparency and based on previous studies (25-28), the PI3K/AKT pathway serves a key role in regulating inflammatory responses and tissue repair. Proteomic analysis showed increased abundance of FAK- and PI3K-related proteins in GA-treated corneas, indicating that the FAK/PI3K/AKT pathway may contribute to GA-mediated corneal repair.

Therefore, both the corneal alkali-burn model and NaOH-induced HCECs were employed in subsequent experiments to further validate the regulatory effects of GA on the PI3K/AKT signaling pathway *in vivo* and *in vitro*, aiming to clarify the molecular mechanisms underlying corneal repair and anti-angiogenic activity.

Network pharmacology analysis of potential targets and mechanisms of GA in improving corneal alkali burn. Network pharmacology has emerged as a powerful approach for identifying potential targets and elucidating the signaling pathways of bioactive compounds in traditional Chinese medicine (29,30). To further investigate the molecular mechanisms by which GA regulates CNV following alkali burn injury, a

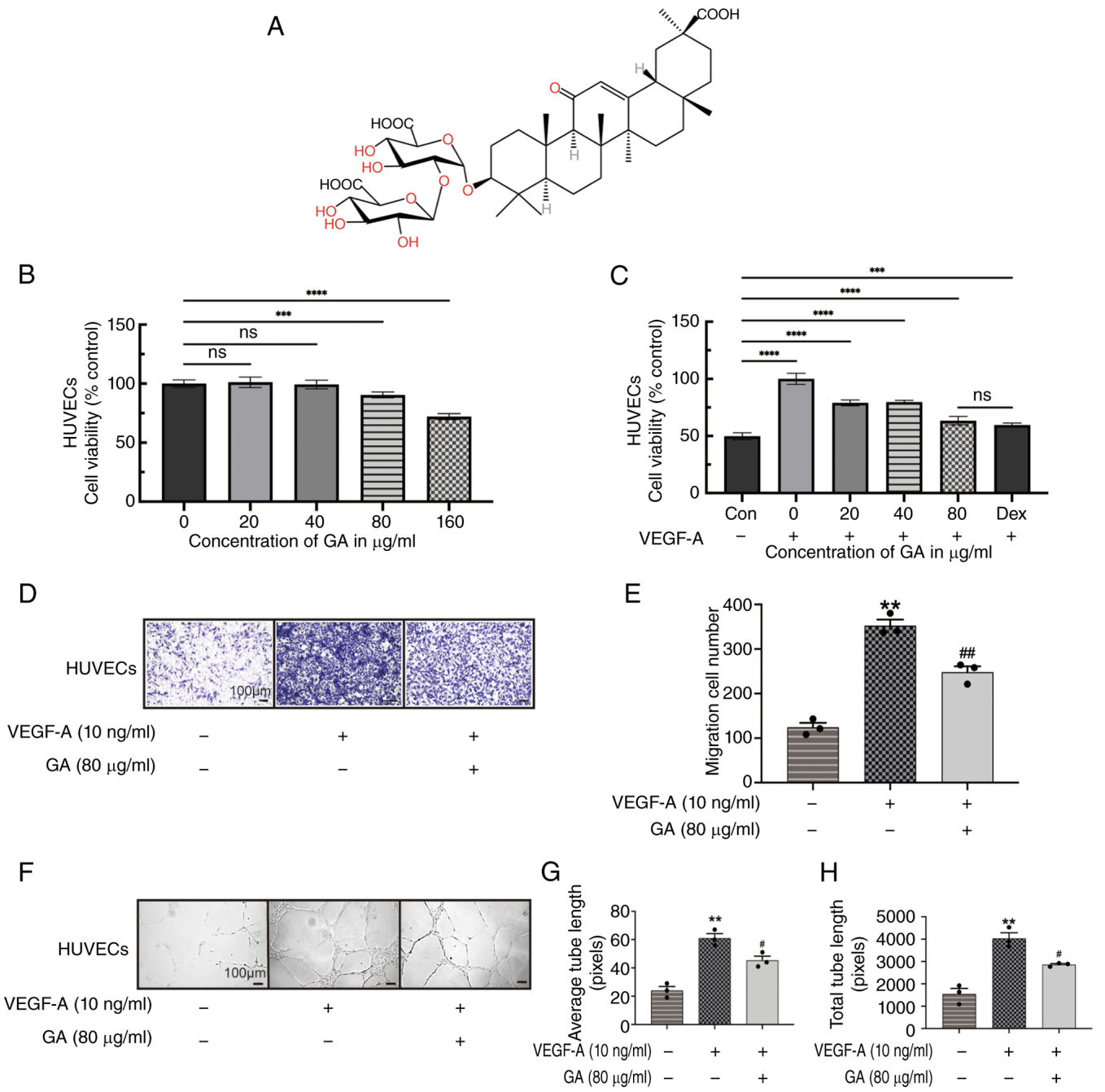

Figure 2. GA suppresses VEGF-A-induced migration and angiogenesis in HUVECs. Transwell migration and tube formation assays were used to evaluated endothelial cell function. (A) Chemical structural formula of GA. (B) HUVECs were incubated with GA at concentrations ranging from 0-160 μg/ml for 48 h. Cell viability was detected via the CCK-8 kit; a quantitative histogram of the viability data is shown. (C) CCK-8 assay showing that GA (0-80 μg/ml) and the positive control, Dex, reversed the viability increase triggered by 10 ng/ml VEGF-A; the corresponding quantitative bar graph is included. (D) Representative Transwell cell migration assay. (E) Quantitative analysis of Transwell cell migration. (F) Representative tube formation assay. (G) Quantitative analysis of average tube length in tube formation assay. (H) Quantitative analysis of total tube length in tube formation assay. Scale bars: 100 μm. Data are presented as means ± SD (n=3). ns, not significant; **P<0.01; ***P<0.001; ****P<0.0001 vs. NC group; $^{\#}$P<0.05 and $^{\#\#}$P<0.01 vs. VEGF-A group. GA, glycyrrhizic acid; VEGF-A, vascular endothelial growth factor A; HUVECs, human umbilical vein endothelial cells; Dex, dexamethasone.

network pharmacology-based strategy was applied to screen and analyze potential targets and signaling pathways associated with GA.

Potential targets of GA were predicted using multiple databases, including BATMAN (probability ≥50%), PharmMapper (score ≥0.5), TargetNet (score ≥0.5) and SwissTargetPrediction (probability >0). After removing duplicate entries, 389 candidate targets were identified (Fig. 5A). Disease-related targets associated with 'corneal alkali burn' were retrieved from the GeneCards database (score >1), yielding 244 disease targets. The intersection of the two datasets identified 43 potential overlapping targets that may mediate the therapeutic effects of GA on corneal alkali burn (Fig. 5C). KEGG pathway enrichment analysis of these 43 targets revealed that the top 30 markedly enriched pathways included the PI3K/AKT signaling pathway, consistent with previous proteomic findings (Fig. 5B). Based

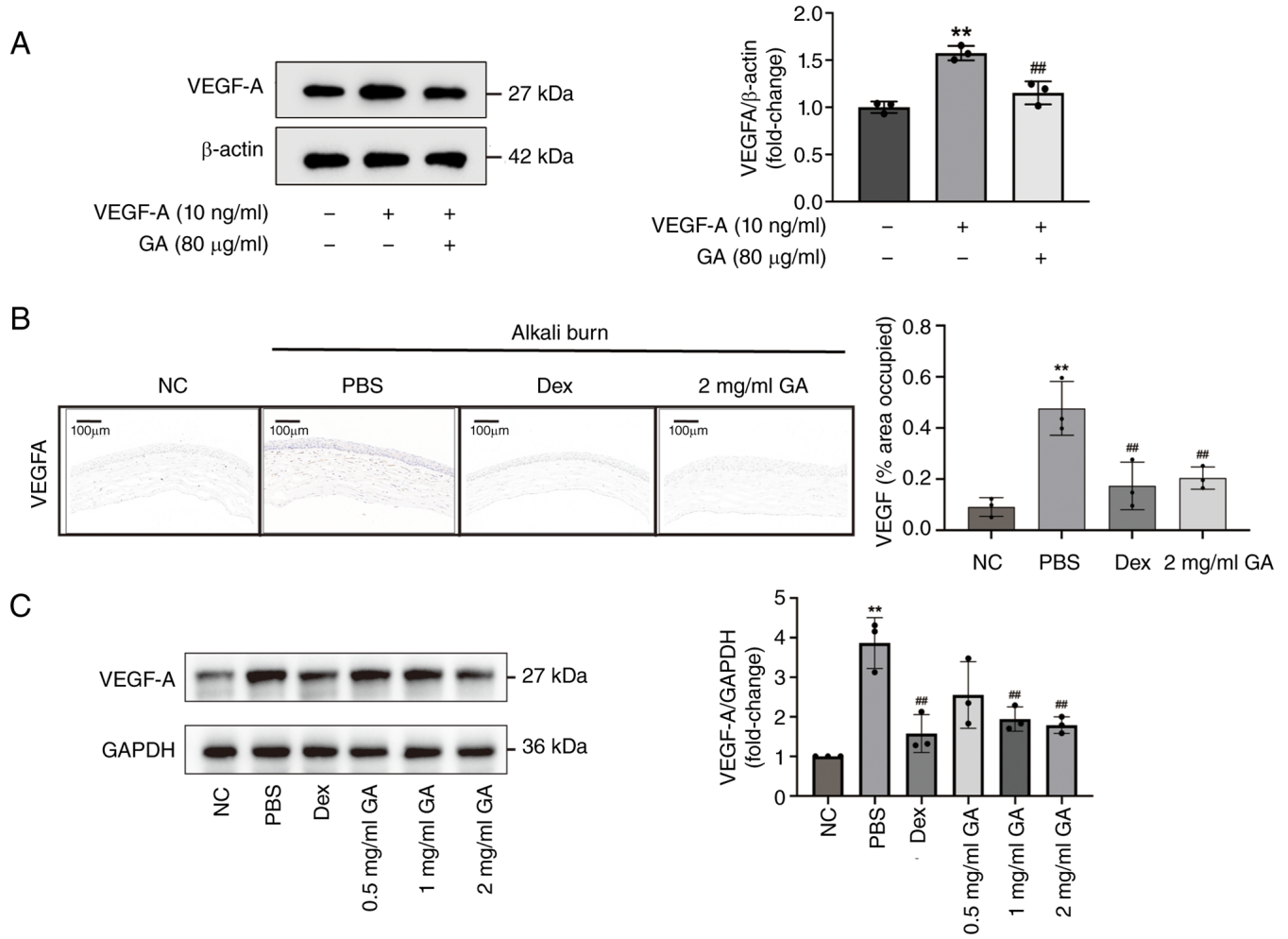

Figure 3. GA suppresses VEGF-A expression *in vivo* and *in vitro*. (A) Western blotting and quantitative analyses of VGEF-A expression in HUVECs. (B) Expression of VEGF-A determined using immunohistochemistry. (C) Western blotting and quantitative analyses of VGEF-A expression in cornea tissue. Data are presented as means ± SD (n=4). ns, not significant; **P<0.01 vs. NC group; $^{\#\#}$P<0.01 vs. VEGF-A group. GA, glycyrrhizic acid; VEGF-A, vascular endothelial growth factor A; HUVECs, human umbilical vein endothelial cells; Dex, dexamethasone.

on these results, a compound-target-pathway-disease network was constructed using the core pathways, key targets and bioactive compound (Fig. 5D). The network comprised 75 nodes and 241 edges, representing 43 targets, 30 signaling pathways and one compound. The color intensity of the nodes corresponded to their degree values, where higher degree values indicate greater importance within the network.

Finally, molecular docking analysis was performed to evaluate the binding affinity between GA and the core targets associated with corneal alkali burn (Fig. 5E). The binding energy was used to estimate the stability and strength of the ligand-protein interactions. Generally, a binding energy ≤-5.0 kcal/mol indicates good binding activity, whereas a binding energy ≤-7.5 kcal/mol reflects strong binding affinity. The visualized docking interactions are presented in Fig. 5F.

The present study intersected the DEPs identified through quantitative proteomics with candidate targets predicted via network pharmacology and the two shared core positive proteins, albumin (ALB) and plasminogen (PLG), were screened for cellular validation using western blotting assays. The western blotting results confirmed that protein levels of ALB and PLG in HCECs were markedly upregulated in the GA-treated group compared with those in the alkali-injured model group, which validated the reliability of the DEPs screened through proteomics and the target prediction results of network pharmacology. Mechanistically, ALB neutralizes toxic oxidized lipids, eliminates reactive oxygen species and stabilizes epithelial junctions to suppress inflammatory infiltration. PLG participates in extracellular matrix remodeling and facilitates epithelial cell migration, thereby accelerating the healing of alkali-induced corneal wounds. Moderate upregulation of PLG expression by GA maintains physiological fibrinolytic balance and avoids excessive degradation of the corneal stroma. Collectively, ALB and PLG synergistically restore the activity of the protective FAK/PI3K/AKT signaling cascade, thereby alleviating alkali-triggered corneal injury and restraining pathological CNV. The western blotting verification data for ALB and PLG are presented in Fig. S1.

GA inhibits apoptosis in corneal epithelial cells. To clarify the mechanism underlying how GA attenuates corneal epithelial-cell apoptosis, we assessed the expression of key apoptosis regulators (Bax, Bcl-2 and caspase-3). Alkali burn markedly

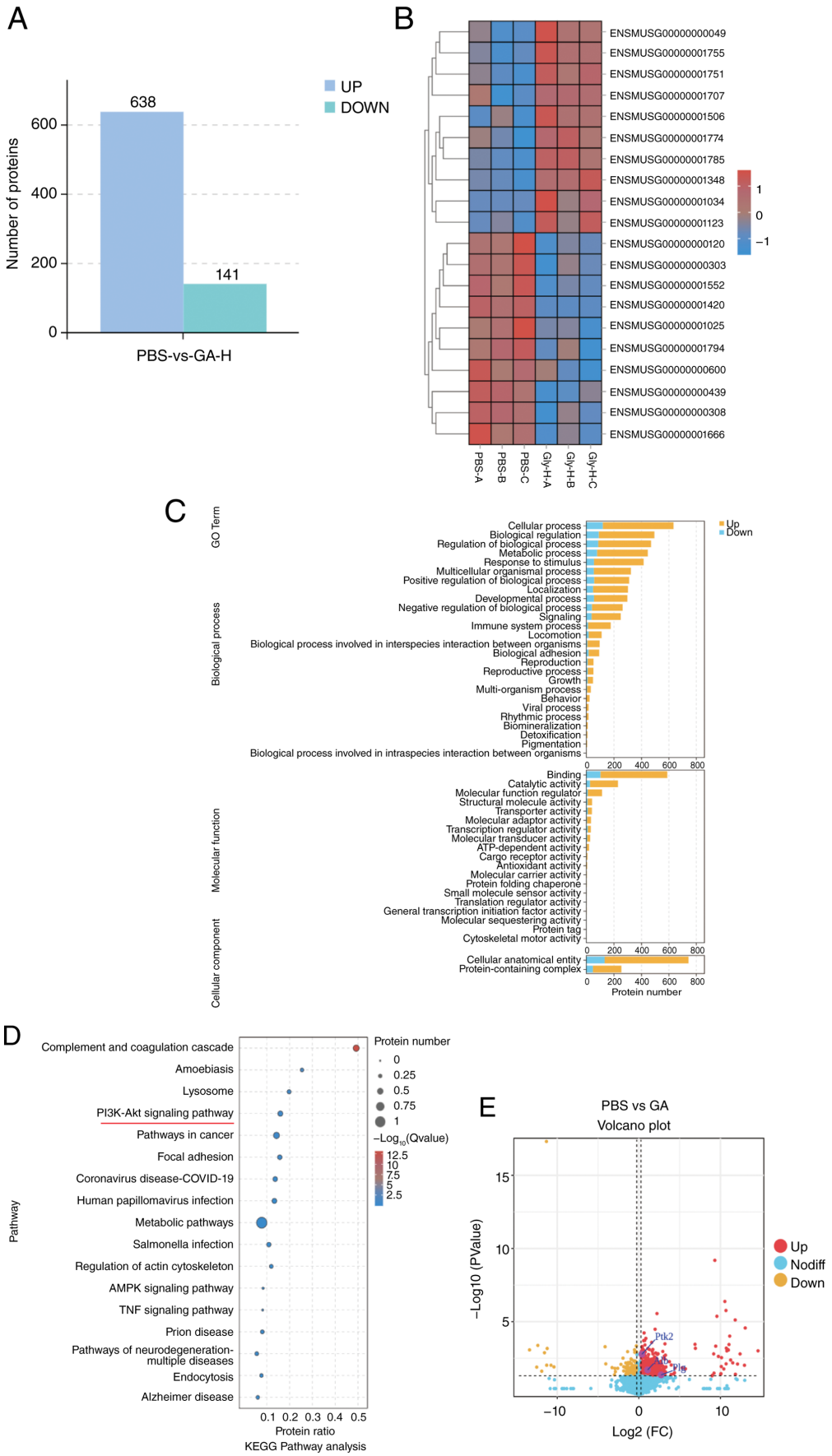

Figure 4. DIA-based quantitative proteomic analysis results. (A) Statistical chart of different protein changes in the PBS and GA groups. (B) Heatmap of the top 20 differentially expressed proteins in the PBS and GA groups. (C) GO enrichment of those commonly selected differential proteins in the PBS and GA groups, including the molecular function, cellular component and biological process categories. (D) Bubble diagram of the KEGG pathway analysis. (E) Volcano map of the differentially expressed proteins in the PBS and GA groups. DIA, data-independent acquisition; GA, glycyrrhizic acid; GO, Gene Ontology; KEGG, Kyoto Encyclopedia of Genes and Genomes.

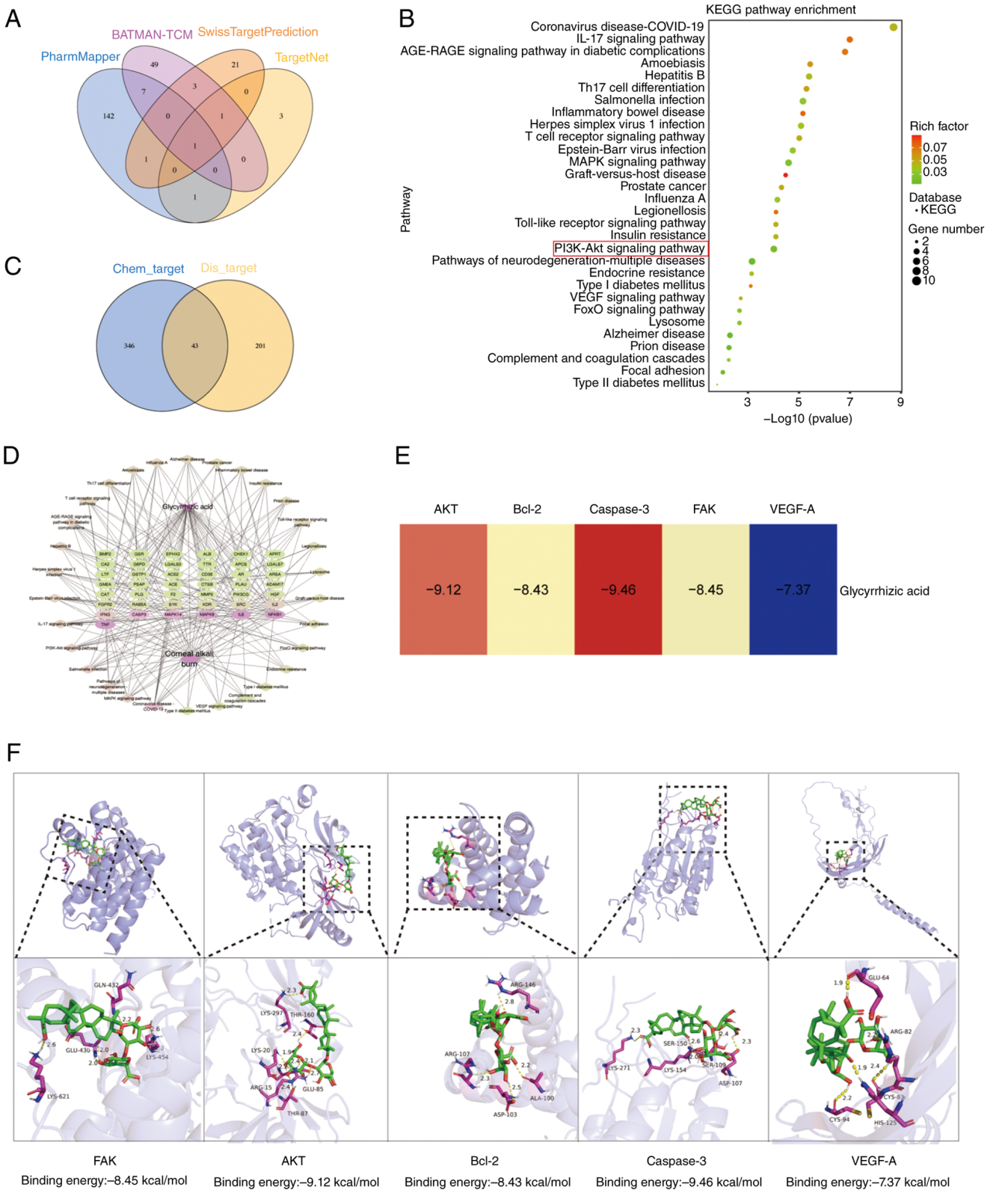

Figure 5. Network pharmacology analysis of the compounds of GA combined with corneal alkali burns. (A) Intersection of targets among the different databases. (B) Bubble chart of the top 30 KEGG pathways. (C) Venn diagram. (D) Compound-target-pathway-disease network diagram. (E) Thermal energy diagram of the protein targets and active ingredient docking. (F) Molecular docking of the representative compounds with protein targets. The figure was created and edited using Adobe Illustrator. GA, glycyrrhizic acid; KEGG, Kyoto Encyclopedia of Genes and Genomes; CASP3, caspase-3; FAK, focal adhesion kinase; VEGF-A, vascular endothelial growth factor A.

increased pro-apoptotic Bax and caspase-3 expression levels while decreasing those of anti-apoptotic Bcl-2 compared with the expression levels measured in the normal control (Fig. 6A and B). GA treatment effectively reversed these changes, with the most potent anti-apoptotic effect observed at 2 mg/ml.

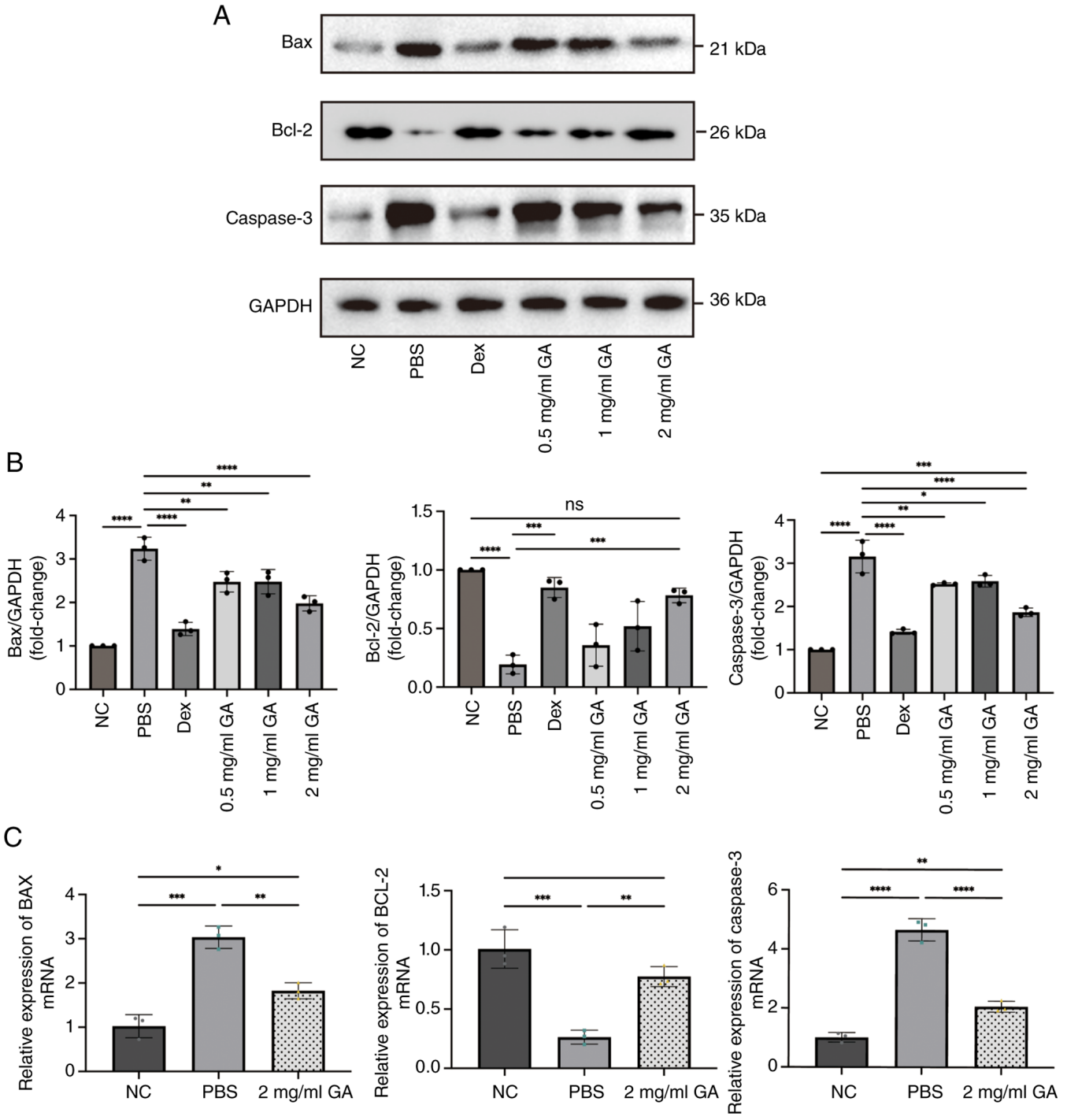

Figure 6. GA inhibited corneal cell apoptosis in alkali burn mice. (A) Western blotting and (B) quantitative analyses of Bax, Bcl-2 and caspase-3 expression in the mice. (C) The mRNA expression of Bax, Bcl-2 and caspase-3 in the three experimental groups were analyzed via qPCR. Data are presented as means ± SD (n=3). ns, not significant; *P<0.05; **P<0.01; ***P<0.001; ****P<0.0001. GA, glycyrrhizic acid; NC, negative control.

Collectively, these results suggested that GA exerts a protective effect against alkali burn-induced corneal epithelial injury by modulating apoptosis-related signaling pathways and inhibiting excessive cell apoptosis.

GA promotes proliferation and migration while inhibiting HCEC apoptosis by activating the FAK/PI3K/AKT signaling pathway. To evaluate the effects of GA on HCEC viability, its cytotoxicity at different concentrations was initially determined using the CCK-8 assay. The results showed that GA had no significant effect on cell viability within the concentration range of 0-200 μg/ml; however, a notable decrease in cell viability was observed at 400 μg/ml (P<0.05; Fig. 7A). Subsequently, HCECs were exposed to 6 mM NaOH for 50 sec to establish a corneal injury model and then co-incubated with GA (0-300 μg/ml) to determine the optimal treatment concentration. The results indicate that 250 μg/ml GA provided the most pronounced protective and proliferative effects on NaOH-damaged cells; hence, this concentration was chosen for subsequent experiments

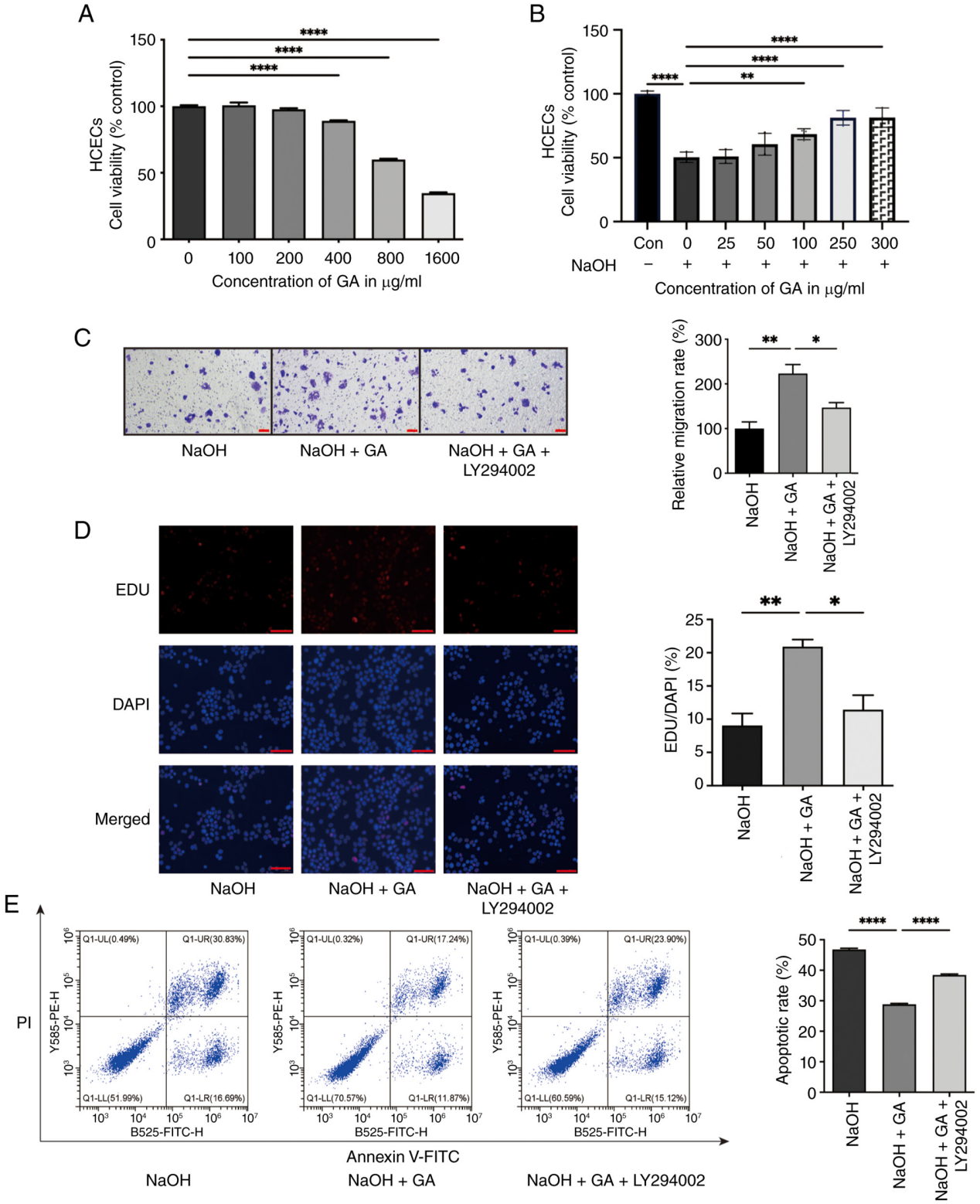

Figure 7. GA enhances HCEC migration, promotes epithelial repair and activates the FAK/PI3K/AKT signaling pathway. (A) HCECs were treated with increasing concentrations of GA (0-1,600 μg/ml) for 24 h and cell viability assessed using the CCK-8 assay. (B) Determination of the optimal GA treatment concentration in NaOH-injured HCECs using the CCK-8 assay. (C) Invasive capacity of HCECs was evaluated using Transwell assays (scale bar, 100 μm). (D) Proliferation of HCECs was assessed via EdU staining. (E) Flow cytometric analysis of apoptosis in each treatment group, showing representative scatter plots and quantification of apoptotic cell percentages. Data are presented as means ± SD (n=3). ns, not significant; *P<0.05; **P<0.01; ****P<0.0001. GA, glycyrrhizic acid; HUVECs, human umbilical vein endothelial cells; FAK, focal adhesion kinase.

(Fig. 7B). Transwell migration and EdU proliferation assays revealed that GA markedly enhanced the migratory and proliferative ability of HCECs, whereas these effects were markedly attenuated by co-treatment with a PI3K inhibitor (Fig. 7C and D). In addition, flow cytometric analysis demonstrated that GA effectively reduced NaOH-induced apoptosis

in HCECs, whereas the inhibition of PI3K reversed this effect and increased the apoptotic rate (Fig. 7E).

To clarify whether the anti-neovascularization effect of GA relies on the FAK/PI3K/AKT signaling pathway and identify the upstream-downstream order of VEGF-A and PI3K, the present study performed western blotting-based PI3K inhibitor (LY294002) rescue assays in alkali-stimulated HCECs. Consistent with previous data, GA intervention elevated phosphorylated FAK, PI3K and AKT levels, whereas co-treatment with LY294002 markedly abolished the activation of PI3K/AKT without altering VEGF-A expression. These results indicated that LY294002 blocks downstream PI3K/AKT signaling but does not reverse GA-mediated VEGF-A suppression, suggesting that the inhibitory effect of GA on VEGF-A is largely independent of PI3K/AKT activation.

Combined with the functional data showing that GA inhibits VEGF-A-induced angiogenesis in HUVECs, the present study confirmed that GA exerts anti-CNV effects by primarily repressing VEGF-A production and that the FAK/PI3K/AKT pathway acts as a downstream effector mediating epithelial-protective functions rather than as an upstream regulator of VEGF-A (Fig. 8A-B). Moreover, GA treatment markedly increased FAK, PI3K and AKT phosphorylation, with a concomitant upregulation of the downstream targets, Bcl-2 and cyclin D1. By contrast, co-treatment with the PI3K inhibitor markedly attenuated these effects. (Fig. 8C-I).

Overall, GA promotes the proliferation and migration of NaOH-injured HCECs and inhibits apoptosis by activating the FAK/PI3K/AKT pathway, thereby exerting cytoprotective effects during corneal injury repair.

Discussion

The cornea is an avascular and transparent tissue and its structural integrity is essential for visual acuity. Under pathological conditions, such as infection, trauma, or corneal transplantation, multiple insults can trigger CNV and fibrotic scarring, thereby compromising transparency. Alkali burn induces an acute and pronounced inflammatory response characterized by limbal vasodilation, increased vascular permeability, infiltration and migration of inflammatory cells and activation of the vascular endothelium, all of which promote neovessel formation (31,32). Large numbers of pro-inflammatory cells (such as macrophages and neutrophils) accumulate at the injury site; classically activated M1 macrophages secrete IL-1β, IL-6, TNF-α and VEGF-A, driving endothelial proliferation and sprouting (33). In addition, IL-1β, IL-1α, interferon-γ and TNF-α can induce apoptosis and impede tissue repair (34-36). Thus, effective therapeutic strategies should concurrently target inflammation and apoptosis. Using a murine alkali-burn model, the present study systematically assessed the effects of GA on corneal inflammation and CNV. GA markedly attenuated inflammatory changes, reduced corneal haze and suppressed CNV while mitigating tissue injury by upregulating cyclin D1 and Bcl-2 expression and downregulating that of Bax and caspase-3. These data suggest that the protective actions of GA are closely associated with activation of the FAK/PI3K/AKT signaling axis (Fig. 9).

GA, a triterpenoid saponin extracted from *Glycyrrhiza* roots and rhizomes, is a principal bioactive constituent exhibiting anti-inflammatory, antioxidative and immunomodulatory properties, as well as a favorable safety profile. Previous studies reported no apparent toxicity of GA <200 μg/ml in macrophages (37) and a safety range of 12.5-300 μg/ml in AEC II cells (38). Consistently, the present study found that ≤80 μg/ml GA was safe and effective in HUVECs, whereas 250 μg/ml was optimal in HCECs.

Alkali burn commonly resulted in epithelial loss, stromal edema, CNV and decreased transparency, which is consistent with prior reports (5). The therapeutic efficacy observed in the present study was evaluated using corneal opacity scores and CNV grading, with Dex serving as a positive control. As a commonly used corticosteroid for ocular surface disease, Dex suppresses local inflammation and helps preserve transparency (39). GA achieved Dex-comparable effects in reducing edema by inhibiting CNV and lymphangiogenesis, indicating that GA may act as a natural anti-inflammatory agent with glucocorticoid-like benefits.

Inflammation-driven angiogenesis is dependent on the interplay between inflammatory cells and angiogenic mediators. Alkali injury promotes neutrophil and macrophage infiltration and enhances the secretion of pro-angiogenic factors, such as VEGF, further amplifying inflammation (40). Persistent elevation of IL-6 and TNF-α levels facilitates epithelial migration, proliferation and tissue remodeling (41). In the model of the present study, GA markedly reduced the levels of IL-6, TNF-α, IL-17 and VEGF in corneal tissues, consistent with published observations (42). FAK, which is encoded by *PTK2*, functions as a non-receptor tyrosine kinase that orchestrates key cellular processes. Aberrant FAK activation correlates with enhanced proliferation and migration and could serve as a promising therapeutic target for various diseases (43). The proteomic and bioinformatic analyses revealed that GA-responsive DEPs were markedly enriched in the PI3K/AKT pathway, with a notable upregulation of FAK and PI3K detected in GA-treated corneas. Network pharmacology and molecular docking further indicated high binding affinities between GA constituents and proteins related to FAK and the PI3K/AKT cascade, suggesting FAK is a putative target of GA.

The PI3K/AKT pathway governs cell proliferation, migration, metabolism and survival (44) and GA modulates this pathway in a context-dependent manner across disease models. For example, GA suppresses IL-1β-induced PI3K/AKT and NF-κB signaling, thereby attenuating inflammation (45); in acute liver injury, GA inhibits HMGB1 and PI3K/mTOR signaling to reduce inflammatory cytokine release and apoptosis (46); in LPS-stimulated RAW264.7 cells, GA and its derivative, 18β-glycyrrhetinic acid, target PI3K p110δ/γ isoforms, suppress NF-κB activation and lower TNF-α, IL-6 and IL-1β secretion in a dose-dependent manner (47). Tsai *et al* (48) reported that GA restrains tumor growth and migration in hepatocellular models by modulating ERK, AKT and EGFR signaling, consequently triggering caspase-8/9-mediated mitochondrial apoptosis. In a rat model of colitis-associated cancer, GA downregulated NF-κB, COX-2, iNOS and VEGF expression, thereby reducing inflammation, aberrant proliferation and angiogenesis (49).

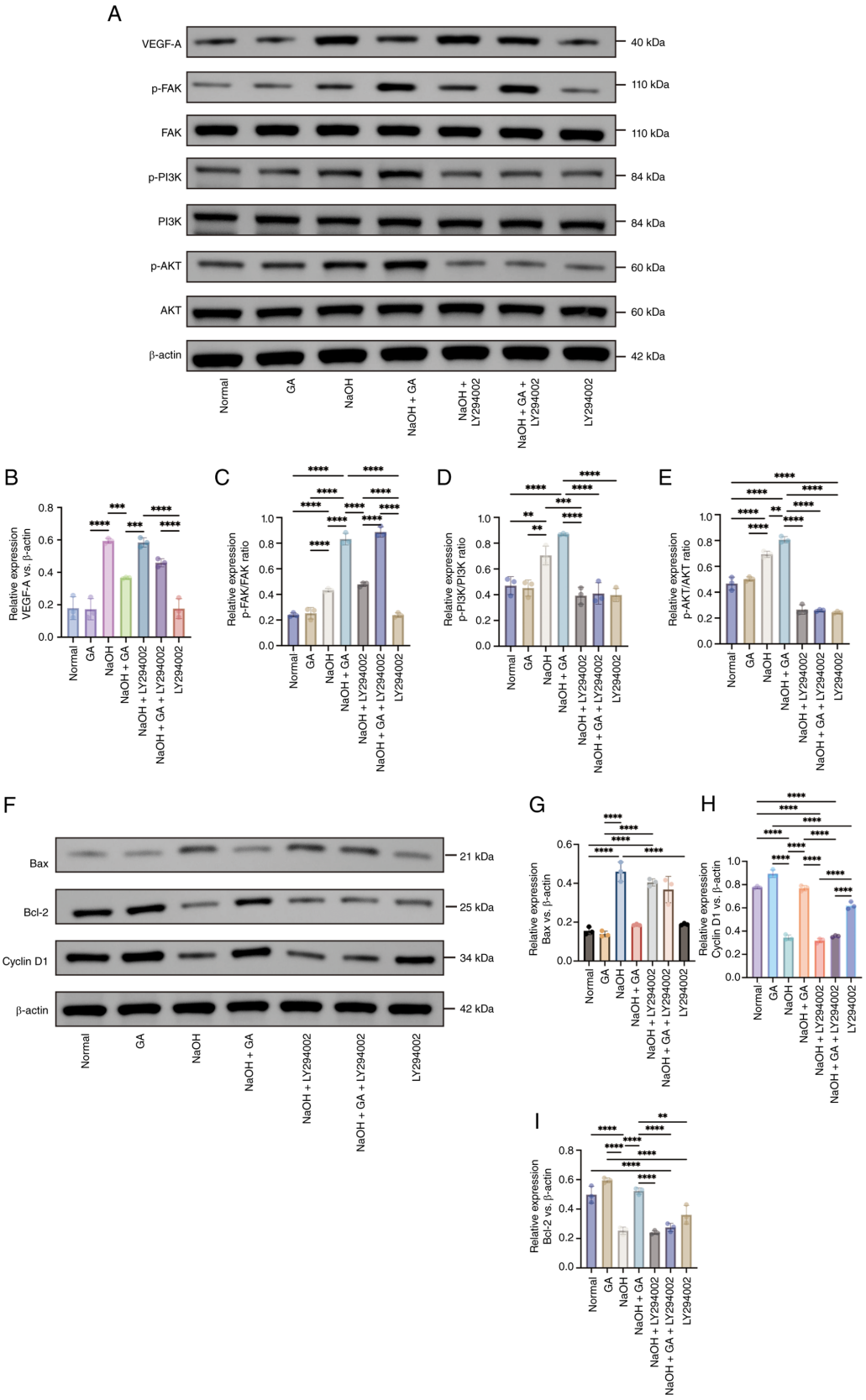

Figure 8. PI3K inhibitor rescue assays clarified the hierarchical relationship between VEGF-A and the FAK/PI3K/AKT pathway in alkali-injured HCECs. (A) Representative western blot bands showing the protein expression levels of VEGF-A, p-FAK, FAK, p-PI3K, PI3K, p-AKT, AKT and the internal reference (β-actin) across seven experimental groups: Normal, GA, NaOH, NaOH + GA, NaOH + LY294002, NaOH + GA + LY294002 and LY294002 alone. (B) Quantitative grayscale analysis of relative VEGF-A expression normalized to β-actin. Quantitative grayscale analysis of (C) p-FAK/FAK ratio. (D) p-PI3K/PI3K ratio. (E) Quantitative grayscale analysis of the p-AKT/AKT ratio. (F) Western blotting detection of Bax (apoptosis-related protein), Bcl-2 (anti-apoptotic protein) and cyclin D1 (proliferation marker) in the Normal, GA, NaOH, NaOH + GA, NaOH + LY294002, NaOH + GA + LY294002 and LY294002 alone. Statistical quantification of (G) Bax, (H) Bcl-2 and (I) cyclin D1 expression normalized to that of β-actin. Data are presented as mean ± SD (n=3). **P<0.01; ***P<0.001; ****P<0.0001. VEGF-A, vascular endothelial growth factor A; FAK, focal adhesion kinase; HUVECs, human umbilical vein endothelial cells; p-, phosphorylated; GA, glycyrrhizic acid.

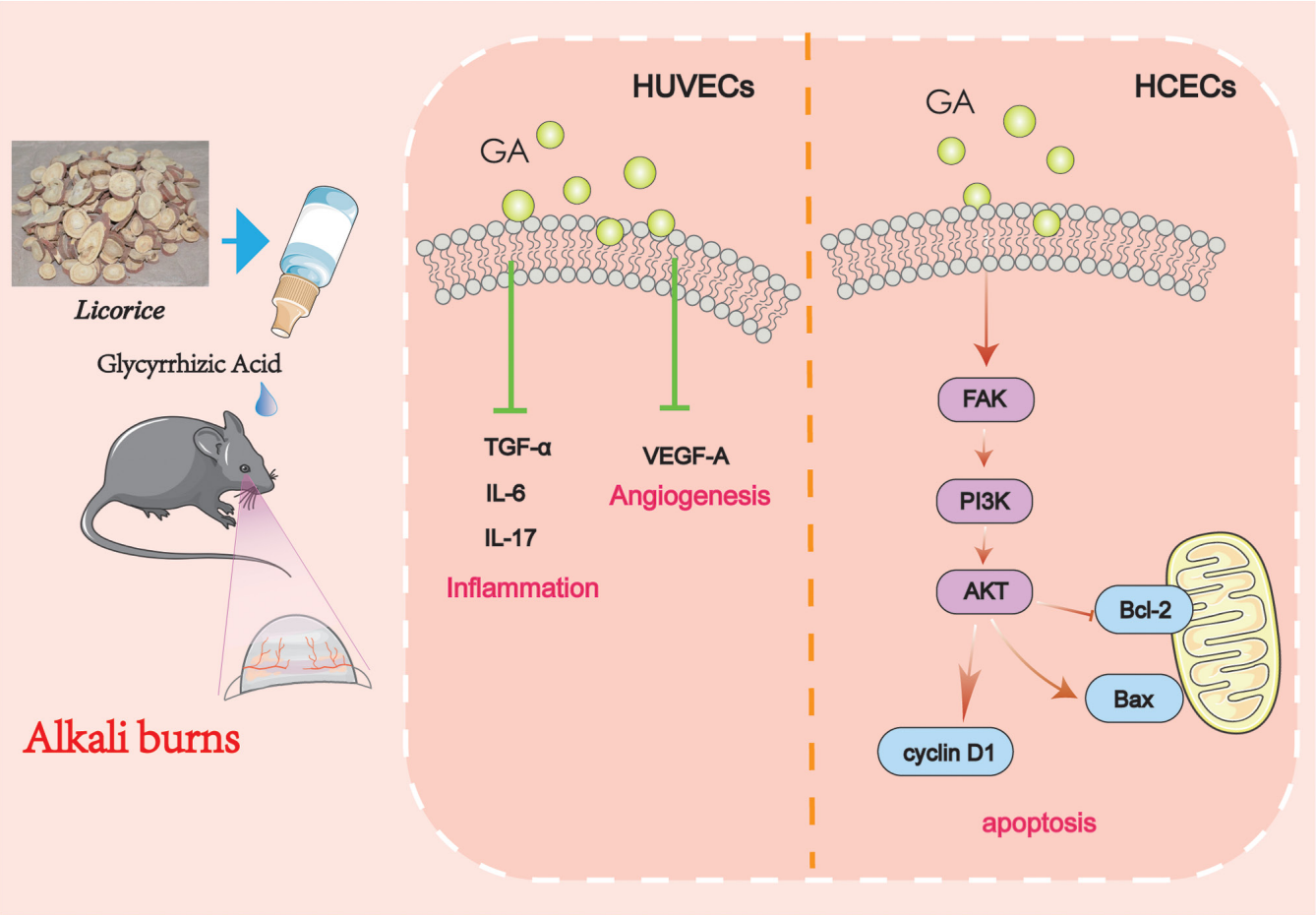

Figure 9. Proposed mechanism of GA in alleviating corneal alkali burn-induced inflammation, angiogenesis and apoptosis. The figure was created and edited using Adobe Illustrator. GA, glycyrrhizic acid; TGF, transforming growth factor; VEGF-A, vascular endothelial growth factor A; HUVEC, human umbilical vein endothelial cells; HCEC, human corneal epithelial cells; FAK, focal adhesion kinase; PI3K, phosphoinositide 3-kinase; AKT, protein kinase B; Bcl-2, B-cell lymphoma-2; Bax, Bcl-2-associated X protein; cyclin D1, cyclin D1.

Collectively, these studies support the capacity of GA to fine-tune PI3K/AKT signaling.

In ocular disease, the PI3K/AKT pathway status varies by pathology; it is often downregulated in diabetic keratopathy and dry eye but activated in infectious and noninfectious keratitis (50). In the healthy corneal epithelium, low PI3K/AKT activity maintains homeostasis. Upon injury, growth factors and neuropeptides (such as substance P) activate the PI3K/AKT cascade to promote epithelial proliferation and migration while limiting apoptosis and inflammation, thereby accelerating repair. Hyperglycemia, hyperosmolarity, excess cytokines, toxins and infection disrupt this pathway (51,52). Therefore, targeting the PI3K/AKT pathway represents a promising strategy for corneal repair. In this context, the present study observed that GA upregulated FAK expression and subsequently activated PI3K/AKT signaling, thereby facilitating epithelial regeneration.

To clarify the causal link among GA, VEGF-A and the FAK/PI3K/AKT pathway, PI3K inhibitor rescue assays were conducted in alkali-injured HCECs. Western blotting results showed that LY294002 blocked GA-induced PI3K/AKT activation but had no impact on GA-mediated VEGF-A downregulation, confirming that GA-mediated VEGF suppression is largely independent of PI3K/AKT signaling. Therefore, GA mainly suppresses pathological CNV by reducing VEGF-A expression, whereas activated FAK/PI3K/AKT primarily facilitates epithelial repair and anti-apoptotic effects. GA exerts dual protective effects after corneal alkali injury via this two-tiered regulatory axis. Although PTK2 (FAK) was identified via proteomic analysis and validated *in vitro*, direct assessment of phosphorylated FAK in corneal tissues is warranted.

Apoptosis is critical for corneal homeostasis (53). Bcl-2, a key anti-apoptotic mediator of the intrinsic mitochondrial pathway, functions by heterodimerizing with pro-apoptotic Bax; alterations in its expression can influence epithelial cell lifespan and turnover (54). Activation of caspase-3 is a hallmark of apoptosis (55) and reduced Bcl-2 expression generally correlates with increased apoptotic activity (56). The anti-apoptotic capacity of GA has been documented previously: in a model of *Mycoplasma gallisepticum* infection, GA suppressed caspase-3/9 activation and upregulated Bcl-2 and Bcl-xL expression (38). Consistent with these findings, the present study's alkali-burn model showed that GA reversed the injury-induced upregulation of Bax and caspase-3 expression and restored that of Bcl-2, confirming its robust anti-apoptotic effect (57). Cyclin D1, which is encoded by *CCND1*, forms active complexes with CDK4/6 to phosphorylate retinoblastoma protein and drive

the G_1-to-S transition (58). Cyclin D1 plays a pivotal role in corneal epithelial proliferation and is notably enriched in the epithelial compartment of pterygium tissues (59); it has also been implicated as a key downstream mediator of nerve growth factor-regulated HCEC proliferation (60). The present data demonstrate, for the first time, that GA promotes corneal epithelial cell proliferation by upregulating cyclin D1 expression through activation of the FAK/PI3K/AKT pathway.

In summary, the present study suggested that GA exerts dual protective effects during corneal alkali burn. On the one hand, GA suppresses VEGF-A expression and thereby inhibits pathological CNV; on the other hand, it activates the FAK/PI3K/AKT pathway to promote epithelial proliferation, migration and survival. These two mechanisms cooperate in facilitating corneal repair. Overall, GA exhibited good safety and biocompatibility at both the cellular and animal levels, supporting its potential as a natural, low-toxicity anti-inflammatory and pro-repair candidate for the treatment of sterile keratitis and related corneal disorders.

The present study systematically demonstrated the protective effects of GA against alkali burn-induced corneal injury. GA exerted its therapeutic actions through multiple coordinated mechanisms. On one hand, GA inhibited VEGF-mediated angiogenesis, thereby effectively suppressing pathological CNV; on the other hand, it modulated the expression of apoptosis-associated molecules, including Bax, Bcl-2 and caspase-3, thereby attenuating corneal epithelial cell apoptosis and promoting tissue repair. Moreover, GA activated the FAK/PI3K/AKT signaling pathway, which contributed to the maintenance of epithelial cell survival and regeneration, ultimately improving the inflammatory microenvironment and restoring corneal structural integrity. In addition, GA exhibited excellent biocompatibility and low cytotoxicity in both corneal tissues and cell models, confirming its favorable safety profile. Collectively, these findings highlighted GA as a naturally derived, multitarget anti-inflammatory and anti-angiogenic compound with promising therapeutic potential. GA may serve as a novel candidate for the prevention and treatment of sterile keratitis, chemical corneal injury and other ocular surface disorders characterized by inflammation and neovascularization.

Acknowledgements

Not applicable.

Funding

The present study was supported by the Jiangsu Provincial Administration of Traditional Chinese Medicine 'Clinical Research on Key Diseases in High-Level Hospital Construction' project (grant no. GSPYY2023009); the Youth project of Wuxi Municipal Health Commission (grant no. Q202348); the Natural Science Foundation of Nanjing University of Chinese Medicine (grant no. XZR2024316); and the Nantong Municipal Guiding Project of Science and Technology Plan (grant no. MSZ2025081).

Availability of data and materials

The data generated in the present study may be requested from the corresponding author.

Authors' contributions

JY conceived the study, prepared all figures, wrote the original draft and performed the investigation. HQ was responsible for analyzing the data, designing the methodology, preparing all figures and writing the original draft. YF was responsible for conceptualization of the study, organising raw experimental data and preparing all figures. WX conceived the study and constructed figures. NW performed the experiments and analyzed data. ND was responsible for organising raw experimental data and designing the methodology. JJ was responsible for conceptualization of the study, formal analysis of the data, and writing, reviewing and editing of the manuscript. WS conceived and designed the study, interpreted the data, acquired funding, supervised, verified experimental results, and reviewed and edited the manuscript. All authors read and approved the final manuscript. NW and WS confirm the authenticity of all the raw data.

Ethics approval and consent to participate

The present study was approved by the Animals Ethics Committee of the Wuxi Affiliated Hospital of Nanjing University of Chinese Medicine (Wuxi, China; approval no. 2024-171-01). All animal experiments were performed following the ARRIVE guidelines and internationally recognized standards for laboratory animal welfare to reduce distress. This study adhered to the principles of transparency, honesty and integrity in data collection, analysis and reporting.

Patient consent for publication

Not applicable.

Competing interests

The authors declare that they have no competing interests.

References

1. Flaxman SR, Bourne RRA, Resnikoff S, Ackland P, Braithwaite T, Cicinelli MV, Das A, Jonas JB, Keeffe J, Kempen JH, *et al*: Global causes of blindness and distance vision impairment 1990-2020: A systematic review and meta-analysis. Lancet Glob Health 5: e1221-e1234, 2017.
2. Soiberman U, Kambhampati SP, Wu T, Mishra MK, Oh Y, Sharma R, Wang J, Al Towerki AE, Yiu S, Stark WJ and Kannan RM: Subconjunctival injectable dendrimer-dexamethasone gel for the treatment of corneal inflammation. Biomaterials 125: 38-53, 2017.
3. Chen Y, Wang X, Duan Y, Liu L, Chen R, Huang Y, Tan Y, Lu Q, Lin Q and Shen L: Fluorinated ROS-responsive polycation enables noninvasive siRNA delivery for the treatment of corneal neovascularization. Acta Biomater 212: 754-769, 2026.
4. Huang XC, Xu GY, Yang PP, Wang L, Wang H and Hu Y: Recent progress on topical drug therapy for corneal neovascularization. ChemMedChem 20: e202500366, 2025.
5. He M, Li N, Li J and Huang X: Impact of pterygium excision combined with autologous limbal stem cell transplantation on microvascular density, tear film stability, and corneal wound healing. Ann Ital Chir 96: 47-54, 2025.
6. Yang T, Wang X, Guo L, Zheng F, Meng C, Zheng Y and Liu G: Daphnetin inhibits corneal inflammation and neovascularization on a mouse model of corneal alkali burn. Int Immunopharmacol 103: 108434, 2022.

7. Wang K, Jiang L, Zhong Y, Zhang Y, Yin Q, Li S, Zhang X, Han H and Yao K: Ferrostatin-1-loaded liposome for treatment of corneal alkali burn via targeting ferroptosis. Bioeng Transl Med 7: e10276, 2021.
8. Wang Y, Shi S, Zhang L, Wang S, Qin H, Wei Y, Wu X and Zhang M: Imatinib@glycymicelles entrapped in hydrogel: Preparation, characterization, and therapeutic effect on corneal alkali burn in mice. Drug Deliv Transl Res 15: 171-184, 2025.
9. Yu J, Qu H, Xu W, Fang Y, Wang N and Shi W: Mechanisms and therapeutic potential of glycyrrhizic acid: Insights into key signaling pathways and disease modulation (Review). Mol Med Rep 33: 126, 2026.
10. Wang ZY and Nixon DW: Licorice and cancer. Nutr Cancer 39: 1-11, 2001.
11. Citi V, Neggiani F, Sanso M and Calderone V: Pharmacological evaluation of innovative eye drop formulations containing TS-polysaccaride, hyaluronic acid and glycyrrhizin for irritative ocular diseases using in vitro reconstituted human corneal epithelium model. Toxicol In Vitro 75: 105199, 2021.
12. Somayajulu M, McClellan SA, Pitchaikannu A, Bessert D, Liu L, Steinle J and Hazlett LD: Effects of glycyrrhizin treatment on diabetic cornea. J Ocul Pharmacol Ther 37: 12-23, 2021.
13. Hou Y, Xin M, Li Q and Wu X: Glycyrrhizin micelle as a genistein nanocarrier: Synergistically promoting corneal epithelial wound healing through blockage of the HMGB1 signaling pathway in diabetic mice. Exp Eye Res 204: 108454, 2021.
14. Burillon C, Chiambaretta F and Pisella PJ: Efficacy and safety of glycyrrhizin 2.5% eye drops in the treatment of moderate dry eye disease: results from a prospective, open-label pilot study. Clin Ophthalmol 12: 2629-2636, 2018.
15. Ammassam Veettil R, Li W, Pflugfelder SC and Koch DD: A mouse model for corneal neovascularization by Alkali Burn. J Vis Exp: Jun 30, 2023 (Epub ahead of print).
16. Zhang LB, Qiu XY, Zhou YH, Liang ML, Guo L, Qi F, Wu YT, Meng C and Liu GH: Recombinant Sgp130 attenuates alkali-burn cornea through inhibition of IL-6 trans-signaling: From production to therapeutic application. Int J Biol Macromol 377: 153509, 2026.
17. Yan D, Ouyang W, Lin J and Liu Z: Smart coating by thermo-sensitive Pluronic F-127 for enhanced corneal healing via delivery of biological macromolecule progranulin. Int J Biol Macromol 253 (Pt 8): 127586, 2023.
18. Li H, Li J, Hou C, Li J, Peng H and Wang Q: The effect of astaxanthin on inflammation in hyperosmolarity of experimental dry eye model in vitro and in vivo. Exp Eye Res 197: 108113, 2020.
19. Yan D, Yu F, Chen L, Yao Q, Yan C, Zhang S, Wu N, Gong D, Sun H, Fu Y and Shao C: Subconjunctival injection of regulatory T cells potentiates corneal healing via orchestrating inflammation and tissue repair after acute Alkali Burn. Invest Ophthalmol Vis Sci 61: 22, 2020.
20. Yu F, Gong D, Yan D, Wang H, Witman N, Lu Y, Fu W and Fu Y: Enhanced adipose-derived stem cells with IGF-1-modified mRNA promote wound healing following corneal injury. Mol Ther 31: 2454-2471, 2023.
21. Liu Z, Liu K, Shi S, Chen X, Gu X, Wang W, Mao K, Yibulayi R, Wu W, Zeng L, *et al*: Alkali injury-induced pathological lymphangiogenesis in the iris facilitates the infiltration of T cells and ocular inflammation. JCI Insight 9: e175479, 2024.
22. Varinska L, Faber L, Kello M, Petrovová E, Balážová Ľ, Solár P, Čoma M, Urdzík P, Mojžiš J, Švajdlenka E, *et al*: β-Escin effectively modulates HUVECS proliferation and tube formation. Molecules 23: 197, 2018.
23. Matsumoto G, Hirohata R, Hayashi K, Sugimoto Y, Kotani E, Shimabukuro J, Hirano T, Nakajima Y, Kawamata S and Mori H: Control of angiogenesis by VEGF and endostatin-encapsulated protein microcrystals and inhibition of tumor angiogenesis. Biomaterials 35: 1326-1333, 2014.
24. Mazari-Arrighi E, Lepine M, Ayollo D, Faivre L, Larghero J, Chatelain F and Fuchs A: Self-organization of long-lasting human endothelial capillary-like networks guided by DLP bioprinting. Adv Healthc Mater 13: e2302830, 2024.
25. Son KN, Lee SM, Shah D, Chaudhary M, Ong J, Reinhardt C, Shukla D, Han K and Aakalu VK: Histatin-5 improves in vivo corneal wound healing and immunohistochemical neovascular markers after acute Alkali injury. Transl Vis Sci Technol 15: 20, 2026.
26. Chen B, Xu H, Li B, Cai Y, Xie L and Zou J: Targeting LRPPRC to improve corneal wound healing via augmenting autophagy and suppressing TGF-beta/Smad signaling post-alkali burn. J Transl Med 24: 1121, 2026.
27. Guan Y, Jing Y, Yang S, Yan X and Li X: YTHDF1-mediated m6A modification of NREP promotes corneal fibrosis via TGF-β-smad signaling. Invest Ophthalmol Vis Sci 67: 51, 2026.
28. Li Q, Bao Q, Wei C, Xie Y, Zhao S, Yan H, Wu F, Li W, Liu X and Gao H: AIF-1 drives corneal neovascularization by promoting inflammatory macrophage activation via the MAPK and PI3K/AKT/mTOR signaling pathways. Invest Ophthalmol Vis Sci 67: 22, 2026.
29. Nogales C, Mamdouh ZM, List M, Kiel C, Casas AI and Schmidt HHHW: Network pharmacology: curing causal mechanisms instead of treating symptoms. Trends Pharmacol Sci 43: 136-150, 2022.
30. Song S, Wei Q, Tu Y, Zhou S, Zhou J, Tao J, Chen Y, Zhou H and You M: Chlorpyrifos-induced autism and depression-like behaviors are ameliorated by trehalose: Integrating network pharmacology and toxicology analyses and animal experiments. Environ Pollut 393: 127670, 2026.
31. Herbert SP and Stainier DY: Molecular control of endothelial cell behaviour during blood vessel morphogenesis. Nat Rev Mol Cell Biol 12: 551-564, 2011.
32. Gao J, Li J, Liu J, Han R, Chen X, Wang L, Ma Y and Li X: miR-29b-3p promotes the recovery of alkali-burned cornea by targeting Ddx3x. Exp Eye Res 264: 110849, 2026.
33. Yu J, Shen Y, Luo J, Jin J, Li P, Feng P and Guan H: Upadacitinib inhibits corneal inflammation and neovascularization by suppressing M1 macrophage infiltration in the corneal alkali burn model. Int Immunopharmacol 116: 109680, 2023.
34. Horwitz V, Dachir S, Cohen M, Gutman H, Cohen L, Gez R, Buch H, Kadar T and Gore A: Differential expression of corneal and limbal cytokines and chemokines throughout the clinical course of sulfur mustard induced ocular injury in the rabbit model. Exp Eye Res 177: 145-152, 2018.
35. Notara M, Lentzsch A, Coroneo M and Cursiefen C: The role of limbal epithelial stem cells in regulating corneal (Lymph)angiogenic privilege and the micromilieu of the limbal niche following UV exposure. Stem Cells Int 2018: 8620172, 2018.
36. Yang L, Zhang S, Duan H, Dong M, Hu X, Zhang Z, Wang Y, Zhang X, Shi W and Zhou Q: Different effects of pro-inflammatory factors and hyperosmotic stress on corneal epithelial stem/progenitor cells and wound healing in mice. Stem Cells Transl Med 8: 46-57, 2019.
37. Wang BK, Mao YL, Gong L, Xu X, Jiang SQ, Wang YB and Li WF: Glycyrrhizic acid activates chicken macrophages and enhances their Salmonella-killing capacity in vitro. J Zhejiang Univ Sci B 19: 785-795, 2018.
38. Wang Y, Wang L, Luo R, Sun Y, Zou M, Wang T, Guo Q and Peng X: Glycyrrhizic acid against mycoplasma gallisepticum-induced inflammation and apoptosis through suppressing the MAPK pathway in chickens. J Agric Food Chem 70: 1996-2009, 2022.
39. Tan Y, Zhang M, Pan Y, Feng H and Xie L: Suppression of the caspase-1/GSDMD-mediated pyroptotic signaling pathway through dexamethasone alleviates corneal alkali injuries. Exp Eye Res 214: 108858, 2022.
40. Shimizu H, Sakimoto T and Yamagami S: Pro-inflammatory role of NLRP3 inflammasome in experimental sterile corneal inflammation. Sci Rep 9: 9596, 2019.
41. Eslani M, Movahedan A, Afsharkhamseh N, Sroussi H and Djalilian AR: The role of toll-like receptor 4 in corneal epithelial wound healing. Invest Ophthalmol Vis Sci 55: 6108-6115, 2014.
42. Wang P, Hao P, Chen X, Li L, Zhou Y, Zhang X, Zhu L, Ying M, Han R, Wang L and Li X: Targeting HMGB1-NFκb Axis and miR-21 by glycyrrhizin: Role in amelioration of corneal injury in a mouse model of Alkali Burn. Front Pharmacol 13: 841267, 2022.
43. Wang N, Dong SS, Zhuo HF, Wang MW, Xue ZX, Li Z, Meng L, Qi Y, Yuan X and Hu J: Focal adhesion kinase promotes biphasic differentiation and induces infiltration and metastasis of synovial sarcoma. J Transl Med 24: 701, 2026.
44. Yao S, Fu T, Tu Q, Zhang J, Jiang Q, Xu M, Wang Z, Jiao Y and Tian H: IL-17 promotes the phenotypic transformation of vascular smooth muscle cells Through PI3K/AKT signaling pathway. Microcirculation 33: e70050, 2026.
45. Jiang RH, Xu JJ, Zhu DC, Li JF, Zhang CX, Lin N and Gao WY: Glycyrrhizin inhibits osteoarthritis development through suppressing the PI3K/AKT/NF-κB signaling pathway in vivo and in vitro. Food Funct 11: 2126-2136, 2020.
46. Shen CH, Ma ZY, Li JH, Li RD, Tao YF, Zhang QB and Wang ZX: Glycyrrhizin improves inflammation and apoptosis via suppressing HMGB1 and PI3K/mTOR pathway in lipopolysaccharide-induced acute liver injury. Eur Rev Med Pharmacol Sci 24: 7122-7130, 2020.

47. Wang CY, Kao TC, Lo WH and Yen GC: Glycyrrhizic acid and 18β-glycyrrhetinic acid modulate lipopolysaccharide-induced inflammatory response by suppression of NF-κB through PI3K p110δ and p110γ inhibitions. J Agric Food Chem 59: 7726-7733, 2011.
48. Tsai JJ, Pan PJ, Hsu FT, Chung JG and Chiang IT: Glycyrrhizic acid modulates apoptosis through extrinsic/intrinsic pathways and inhibits protein kinase B- and extracellular signal-regulated kinase-mediated metastatic potential in hepatocellular carcinoma in vitro and in vivo. Am J Chin Med 48: 223-244, 2020.
49. Khan R, Rehman MU, Khan AQ, Tahir M and Sultana S: Glycyrrhizic acid suppresses 1,2-dimethylhydrazine-induced colon tumorigenesis in Wistar rats: Alleviation of inflammatory, proliferation, angiogenic, and apoptotic markers. Environ Toxicol 33: 1272-1283, 2018.
50. Chen K, Li Y, Zhang X, Ullah R, Tong J and Shen Y: The role of the PI3K/AKT signalling pathway in the corneal epithelium: Recent updates. Cell Death Dis 13: 513, 2022.
51. Park JH, Moon SH, Kang DH, Um HJ, Kang SS, Kim JY and Tchah H: Diquafosol sodium inhibits apoptosis and inflammation of corneal epithelial cells via activation of Erk1/2 and RSK: In vitro and in vivo dry eye model. Invest Ophthalmol Vis Sci 59: 5108-5115, 2018.
52. Liu Z, Chen D, Chen X, Bian F, Qin W, Gao N, Xiao Y, Li J, Pflugfelder SC and Li DQ: Trehalose induces autophagy against inflammation by activating TFEB signaling pathway in human corneal epithelial cells exposed to hyperosmotic stress. Invest Ophthalmol Vis Sci 61: 26, 2020.
53. Torrealba N, Rodriguez-Berriguete G, Vera R, Fraile B, Olmedilla G, Martínez-Onsurbe P, Sánchez-Chapado M, Paniagua R and Royuela M: Homeostasis: Apoptosis and cell cycle in normal and pathological prostate. Aging Male 23: 335-345, 2020.
54. Robertson DM, Ladage PM, Yamamoto N, Jester JV, Petroll WM and Cavanagh HD: Bcl-2 and Bax regulation of corneal homeostasis in genetically altered mice. Eye Contact Lens 32: 3-7, 2006.
55. Wang H, Zhu J, Jiang L, Shan B, Xiao P, Ai J, Li N, Qi F and Niu S: Mechanism of Heshouwuyin inhibiting the Cyt c/Apaf-1/Caspase-9/Caspase-3 pathway in spermatogenic cell apoptosis. BMC Complement Med Ther 20: 180, 2020.
56. Harada H and Grant S: Apoptosis regulators. Rev Clin Exp Hematol 7: 117-138, 2003.
57. Kossl J, Bohacova P, Hermankova B, Javorkova E, Zajicova A and Holan V: Antiapoptotic properties of mesenchymal stem cells in a mouse model of corneal inflammation. Stem Cells Dev 30: 418-427, 2021.
58. Qie S and Diehl JA: Cyclin D1, cancer progression, and opportunities in cancer treatment. J Mol Med (Berl) 94: 1313-1326, 2016.
59. Kase S, Takahashi S, Sato I, Nakanishi K, Yoshida K and Ohno S: Expression of p27(KIP1) and cyclin D1, and cell proliferation in human pterygium. Br J Ophthalmol 91: 958-961, 2007.
60. Wu D, Qian T, Hong J, Li G, Shi W and Xu J: MicroRNA-494 inhibits nerve growth factor-induced cell proliferation by targeting cyclin D1 in human corneal epithelial cells. Mol Med Rep 16: 4133-4142, 2017.

Copyright © 2026 Yu et al. This work is licensed under a Creative Commons Attribution-NonCommercial-NoDerivatives 4.0 International (CC BY-NC-ND 4.0) License.